

# **Spatial Averaging of Oceanic Rainfall Variability Using Underwater Sound**

## **Ionian Sea Rainfall Experiment 2004: Acoustic Component**

by Jeffrey A. Nystuen<sup>1</sup>, Eyal Amitai<sup>2</sup>, Emmanuel N. Anagnostou<sup>3</sup>,  
and Marios N. Anagnostou<sup>3</sup>

<sup>1</sup> *Applied Physics Laboratory, University of Washington, Seattle, WA*

<sup>2</sup> *George Mason University, Greenbelt, MD*

<sup>3</sup> *University of Connecticut, Storrs, CT*

**Technical Report**  
**APL-UW TR 0701**  
**July 2007**



**Applied Physics Laboratory University of Washington**  
1013 NE 40th Street Seattle, Washington 98105-6698

### *Acknowledgments*

E. Boget designed and deployed the deepwater mooring. The National Observatory of Athens (NOA) made the XPOL radar available to the experiment. G. Chronos at Hellenic Center for Marine Research (HCMR) arranged for the R/V *Philia*, captained by M. Kokos, to deploy and recover the mooring. T. Paganis and A. Gomta, at the Methoni weather station, provided their hand-written data to help interpret the acoustic data. E. Anassontzis, University of Athens, provided logistical support via the NESTOR Institute for Deep Sea Research in Pylos, Greece. The citizens of Finikounda allowed rain gauges to be set up in their yards during the experiment. Funding was provided by the National Science Foundation, Physical Oceanography Division, Grant #0241245.

### *Abstract*

An experiment to evaluate the inherent spatial averaging of the underwater acoustic signal from rainfall was conducted in the winter of 2004 in the Ionian Sea southeast of the coast of Greece. A mooring with four passive aquatic listeners (PALs) at 60, 200, 100, and 2000 m was deployed at 36.85°N, 21.52°E, 17 km west of a dual-polarization X-band coastal radar (XPOL) at Methoni, Greece. A dense rain gauge network was set up in Finikounda, 10 km east from Methoni to calibrate the radar. Eight rain events were recorded during the deployment; six of these events were recorded by both the PALs and the XPOL radar.

The acoustic signal is similar at all depths and rainfall was detected at all depths, although the deeper PALs suffered an unexpected sensitivity loss and consequently did not trigger into high sampling mode as often as the shallower PALs. The total accumulation reported is lower for the deeper PALs. The acoustic signal is classified into wind, rain, shipping, and whale categories. The shipping signal increased throughout the deployment. A signal from whales is present roughly 2% of the time, most often at 200 m, and is consistent with the clicking of deep-diving beaked whales, although there was no visual confirmation of whale presence.

Acoustic co-detection of rainfall with the radar demonstrates the need to classify the rainfall signal in the presence of other underwater noises. Once detection is made, the correlation between acoustic and radar rainfall rates is high. Spatial averaging of the radar rainfall rates in concentric circles over the mooring shows highest correlations with increasing acoustic recording depth, verifying the larger inherent spatial averaging of the rainfall signal with recording depth. For the PAL at 2000 m, the maximum correlation was at 3–4 km, suggesting a listening area for the acoustic rainfall measurement of roughly  $\pi r^2 = 30 - 50 \text{ km}^2$ , in contrast to less than  $3 \text{ km}^2$  for the acoustic measurement at 60 m depth.

## Table of Contents

<b>1. Introduction .....</b>	<b>1</b>
<b>2. Experimental setup .....</b>	<b>2</b>
<b>3. Data collected .....</b>	<b>7</b>
3.1. Acoustic data .....	7
3.2. Radar data .....	8
3.3. Ground validation network .....	9
3.4. Methoni weather station .....	9
<b>4. Acoustic data analysis .....</b>	<b>11</b>
<b>5. Validation of rainfall detection .....</b>	<b>19</b>
5.1. Case Study – 12 February 2004 .....	19
5.2. Case study: Light rain in light wind conditions – 3 and 4 March .....	21
5.3. Case study: Moderate rain in moderate wind conditions – 9 and 12 March .....	22
5.4. Case study: Squall line on 8 March .....	22
<b>6. Spatial averaging of the rainfall signal .....</b>	<b>37</b>
<b>7. Conclusions .....</b>	<b>39</b>
<b>8. References .....</b>	<b>41</b>

This page is intentionally blank.

## 1. Introduction

The ambient sound field in the ocean contains a lot of information about the physical, biological, and anthropogenic processes in the ocean. Interpretation of the ambient sound field can be used to quantify these processes. In particular, rainfall on the sea surface generates a loud and distinctive sound underwater that can be used to detect and quantitatively measure rain at sea (*Ma and Nystuen, 2005*). Furthermore, different raindrop sizes produce distinctive sound underwater, allowing for the inversion of the sound to measurement drop size distribution within the rain (*Nystuen, 2001; Nystuen, 2005*). This allows the potential for rainfall classification at sea using sound (*Nystuen and Amitai, 2003*).

One interesting feature of the acoustical measurement is that the listening area for a hydrophone, its effective ‘catchment basin’, is proportional to its depth, and yet the signal should be independent of depth if the sound source is uniformly distributed on the sea surface. Thus, the acoustical measurement of rainfall has an inherent spatial averaging that can be compared to the beam filling assumption of radar or satellite measurements of rainfall. By making sound measurements at different depths (60, 200, 1000, and 2000 m) and comparing those measurements to simultaneous high-resolution XPOL radar observations, the spatial averaging of the acoustic signal can be explored.

## 2. Experimental setup

In the winter of 2004, an experiment was carried out in the Ionian Sea off the southwestern coast of Greece (Fig. 1). This location offers extremely deep water (over 3 km deep) within the coverage area of coastal radar. The mooring configuration is shown in Fig. 2. Four acoustic sensors were deployed at 60, 200, 1000, and 2000 m depths on a single mooring. The coastal radar was a mobile high-resolution dual-polarization X-band radar (XPOL). The radar was located at Methoni (Fig. 1), 17 km east of the mooring. A dense rain gauge network and a 2-D video disdrometer were deployed at Finikounda, 10 km east of the radar, but in the opposite direction from the mooring. The acoustical measurements and rain gauge network measurements were continuous from mid-January to mid-April, however the radar needed to have an operator present and so its temporal coverage was not continuous. Six precipitation events were captured by all three systems. Table 1 lists the rainfall events that were detected and recorded during the experiment. It also gives the rainfall accumulation totals for each system.

Ocean currents will bend the mooring, causing horizontal displacement of the acoustic sensors. In order to determine this potential displacement, a pressure sensor was placed on the mooring 2 m below the shallowest acoustic recorder. During most of the experiment the mooring line can be assumed to be vertical, but there are a few episodes when the top of the mooring dips and horizontal displacement is assumed to be present. The maximum vertical excursion is 5 m on 5 February, giving the maximum horizontal displacement of the shallowest acoustic recorder as 170 m. The displacements of the deeper recorders will be less. The spatial resolution of the radar (single pixel) is 150 m at the range of the mooring (17 km) and so the mooring can be assumed to be within a single radar range cell throughout the experiment

The temperature and salinity structure of the ocean affect the sound speed profile, which in turn, will cause a refraction of sound. The temperature, salinity, and sound speed structure of the upper 500 m at the mooring site were measured during the deployment (14 January) and recovery (14 April) of the mooring. The water is well mixed to 50 m. There is a layer of warmer and slightly fresher water that is about 130 m thick in January and about 50 m thick in April. This produces a weak sound channel centered at about 150 m deep in January and at about 70 m in April. The sound speed variations associated with these temperatures and salinity structures are potentially important for low-frequency ( $< 2$  kHz) sound traveling at near horizontal grazing angles, but for higher frequency ( $> 5$  kHz)

sound produced at the sea surface (vertical dipole) the refraction of the sound is small and spherical spreading will be assumed.

A sound source at a free surface is an acoustic dipole. Thus the sound intensity recorded at an omnidirectional hydrophone is given by

$$I = \int I_o \cos^2 \theta \text{ atten}(p) dA, \quad (1)$$

where  $I$  is the sound intensity measured at the hydrophone,  $I_o$  is the sound intensity at the surface,  $\cos^2 \theta$  is the directional radiation pattern for a surface source (vertically oriented dipole), and  $\text{atten}(p)$  is the attenuation along the acoustic path  $p$ . The integral is taken over the surface area  $A$ . The attenuation is due to geometric spreading, scattering, and absorption. Scattering is assumed to be negligible. Geometric spreading is affected by the sound speed profile of the ocean. Thus, the attenuation from a surface source to an acoustic recorder is given by

$$\text{atten}(p) = \frac{\exp(-\alpha p)}{r^2 + h^2}, \quad (2)$$

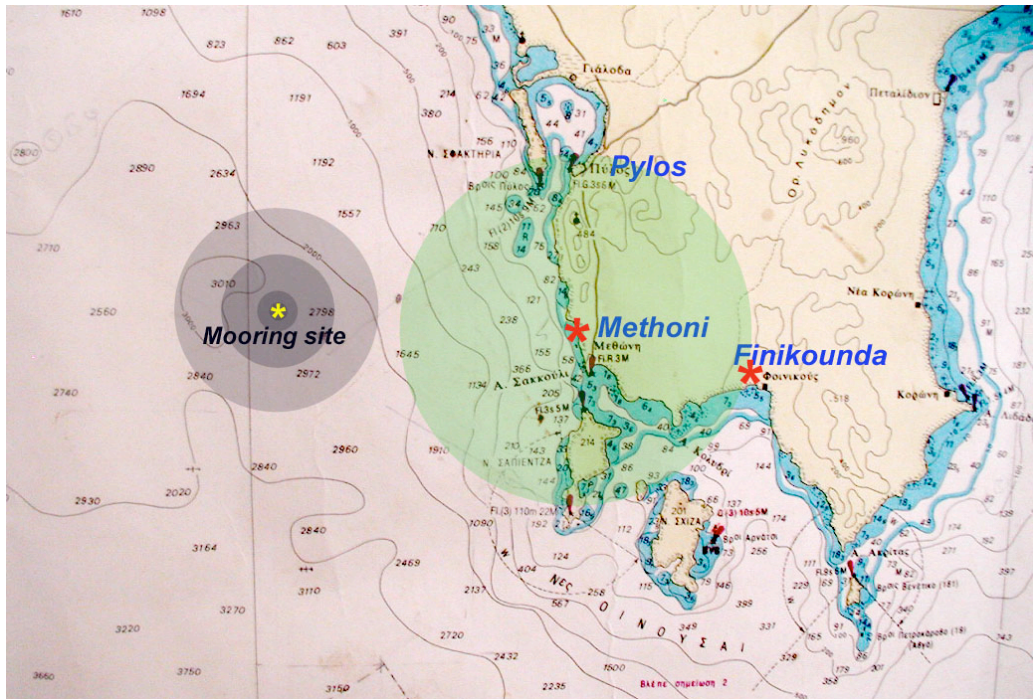
where  $p^2 = r^2 + h^2$ ,  $r$  is the horizontal range to the sound source,  $h$  is the depth of the recorder, and  $\alpha = \alpha(f, S, T)$  is the absorption of sound in seawater and is a function of frequency, salinity, and temperature (*Medwin and Clay*, 1998, p. 109). If one makes the assumption that  $I_o$  is uniform over the sea surface, then Eq. (1) can be used to estimate the effective listening area for each sensor.

Figure 3 shows the fraction of the total energy received as a function of frequency for sensors at 60, 200, 1000, and 2000 m depths. If the listening radius for a sensor is defined as the area receiving 90% of the sound, then the listening radii for the sensors at 2 kHz are 172, 620, 2800, and 5000 m, respectively, roughly three times the depth of the sensor. At 20 kHz the radii are 165, 550, 2000, and 3400 m, respectively. The principal rainfall signal is at 5 kHz. At 5 kHz the radii are 170, 610, 2735, and 4800 m, respectively. Figure 3 also shows the weighting function of the listening radius for a uniform surface source. Within the defined listening area most of the energy is arriving from a much smaller area centered over the mooring. For example, at 5 kHz, 50% of the energy is arriving from the surface area with radii 58, 200, 970, and 1860 m, respectively, which is roughly the depth of the sensor.



**Table 1: Rain events during the deployment. Accumulations are given in mm. \*On March 3<sup>rd</sup> the XPOL was only operational during part of the rain event.**

DATE	PALs				XPOL	Rain Gauges	Methoni Station
	M	N	O	P			
Jan 21/22	68.5	67.5	61.1	52.4	No	No	96.8 mm
Feb 12	13.7	14.6	14.5	11.0	12.1	22.5	20.1
Mar 3	9.9	9.1	9.7	10.3	2.8*	1.0	1.4
Mar 4	4.2	4.2	4.7	3.9	3.6	13.4	13.0
Mar 8	7.0	8.9	12.8	13.4	4.0	11.9	7.9
Mar 9	12.7	11.8	10.7	9.4	13.0	14.1	8.3
Mar 12	29.9	31.2	30.1	23.1	18.1	5.1	5.8
Apr 1	34.0	36.3	31.1	20.1	No	23.5	25.5



**Figure 1. Overview of the experimental site. The mooring location is 17 km west of Methoni. The concentric circles show the nominal listening areas for the four PALs (M, N, O, and P). (The innermost circle is hidden under the symbol.) The X-POL radar is at Methoni. A shaded circle shows 10 km coverage. The dense rain gauge network is at Finikounda.**

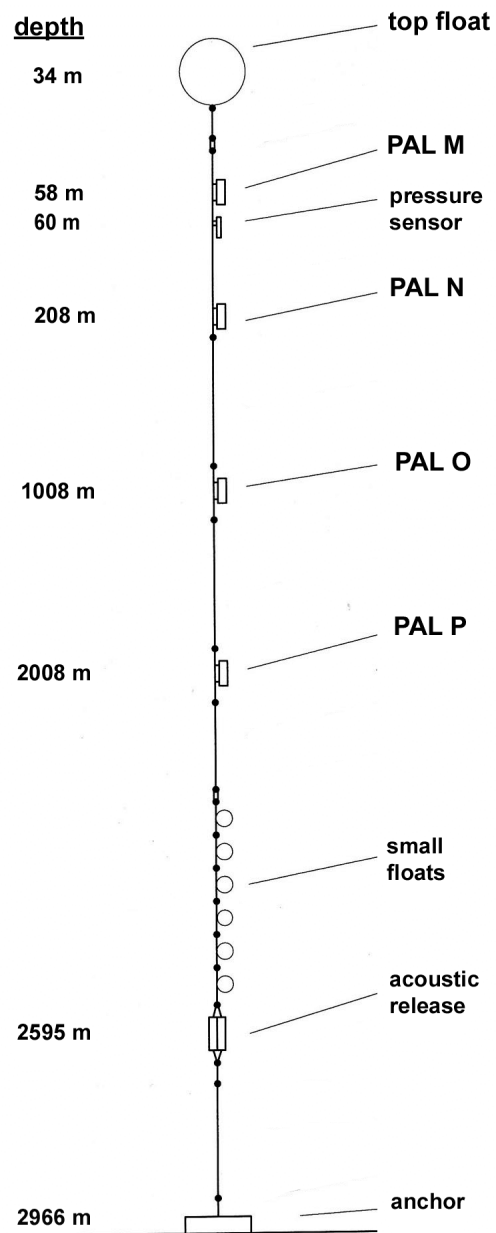


Figure 2. Mooring configuration at 36.85°N, 21.52°E, 17 km west of Methoni, Greece. Four Passive Aquatic Listeners (PALs) are deployed at 58, 208, 1008, and 2008 m, (PALs M, N, O, and P, respectively).

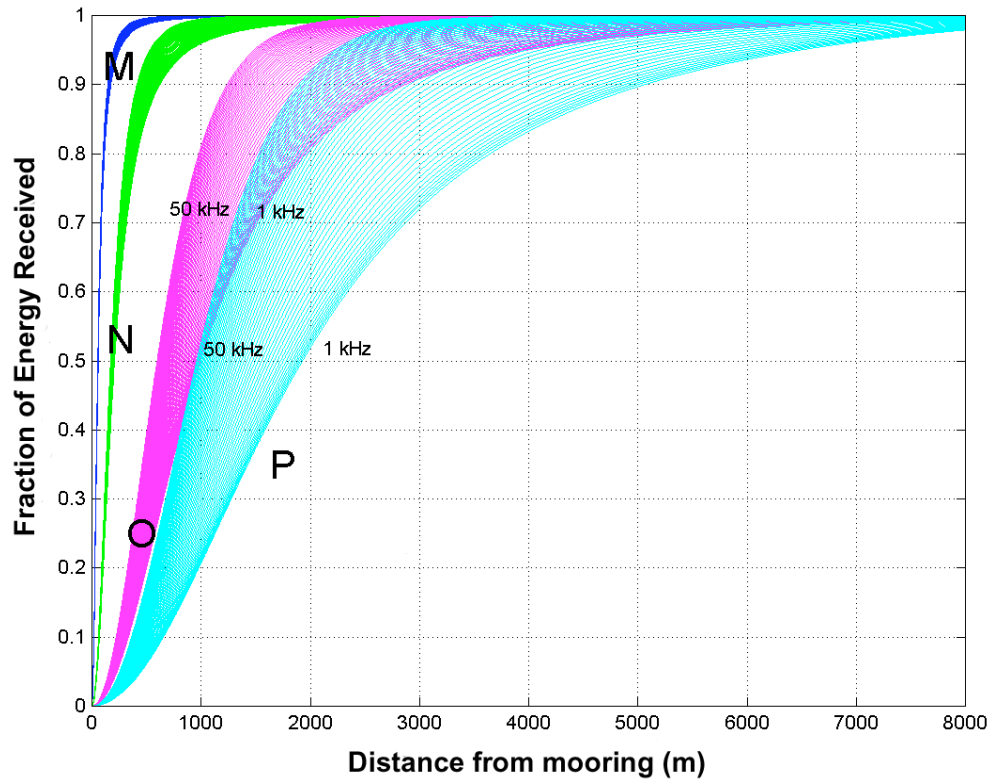


Figure 3. Listening radius for the four PALs (M at 58 m; N at 208 m; O at 1008 m; P at 2008 m) as a function of frequency. The listening radius is reduced at higher frequency by higher absorption of sound. Each group of curves shows this frequency effect from 50 kHz (left) to 1 kHz (right).

### 3. Data collected

#### 3.1. Acoustic data

The acoustic data were collected on four Passive Aquatic Listeners (PALs). PALs consist of a low-noise wideband hydrophone (Hi-Tech-92WB), signal pre-amplifiers, and a recording computer (Tattletale-8). The nominal sensitivity of these instruments is  $-160$  dB relative to  $1 \text{ V}/\mu\text{Pa}$  with an instrument noise equal to an equivalent oceanic background noise level of about  $28$  dB relative to  $1 \mu\text{Pa}^2\text{Hz}^{-1}$ . Band-pass filters are present to reduce saturation from low-frequency sound (high pass at  $300$  Hz) and aliasing from above  $50$  kHz (low pass at  $40$  kHz). The hydrophone sensitivity also rolls off above its resonance frequency, about  $40$  kHz. A further sensitivity correction due to the depth of deployment is also present.

A data collection sequence takes about  $15$  s and consists of four  $10.24$ -ms time series each separated by  $5$  s. Each of these time series is fast Fourier transformed (FFT) to obtain a  $512$ -point ( $0$ – $50$  kHz) power spectrum. These four spectra are spectrally compressed to  $64$  frequency bins, with frequency resolution of  $200$  Hz from  $100$  to  $3000$  Hz and  $1$  kHz from  $3$  to  $50$  kHz. Geophysically generated sounds from rain, drizzle, or wind are generally stationary over a  $15$ -s time interval, whereas banging from ships or moorings, or chirps, whistles or clicks from biological sources are sound signals that usually are non-stationary over a  $15$ -s time interval. Thus, a preliminary evaluation of the sound source is performed by comparing the four spectra from a single data collection sequence. A non-stationary signal is rejected as noise, and another data collection sequence is collected. Otherwise, the four spectra are averaged into a single spectrum that is stored to memory for later analysis. This average spectrum is evaluated to determine the acoustic source (rain, wind, or drizzle) and the source identification is used to set the time interval to the next data collection sequence. For example, if rain is detected, the time interval to the next data collection sequence is set to  $30$  s, whereas if ‘wind’ is detected, the time interval to the next data collection sequence is set to  $5$  min. This allows the PAL to conserve energy between data collection sequences, but maximizes the sampling interval during periods of rainfall.

There is a residual frequency dependent instrument sensitivity that needs to be removed from the data. This is accomplished by assuming that the signal from wind generated wave breaking is a signal with a uniform spectral slope from  $1$  to  $40$  kHz (*Ma and Nystuen, 2005*). At low wind speeds the recorded signal includes

a component from the ambient background and from instrument noise. At high wind speeds, there is a change to the spectral shape of the wind signal due to attenuation of the signal from ambient bubbles in the water. But at moderate wind speeds (4–8 m/s), the sound signal is well above the background noise and has a uniform spectral slope between 1 and 40 kHz. The difference between the observed spectral shape and a uniform spectral slope is assumed to be the frequency dependent sensitivity correction for the PAL. This procedure might remove a real small scale feature of the wind generated sound signal, but such a feature should not be present in the sound signal from a different sound source, such as rain, drizzle, or ships. Thus, the correction procedure is confirmed by examining the data from other sound sources, such as rain, drizzle, or ships, and observing that the spectral features of the sensitivity correction (usually smaller than 1 dB) have been removed.

An unexpected depth dependent sensitivity change was observed, and confirmed by post-experiment testing. Again assuming a uniform sound source at the surface, Eq. (1) predicts a uniform signal with depth, except for the influence of absorption. The absorption of sound in the ocean is known (*Medwin and Clay*, 1998, p. 109) and can be calculated as a function of frequency and depth. Again choosing a sound condition when the signal to noise ratio is high and a uniform surface sound source is expected, for example when the wind speed is 8 m/s, this depth dependent sensitivity change can be detected. Figure 4 shows the mean sound spectra at 8 m/s for each instrument. After adjusting for absorption, a depth dependent offset remains. Between 2 and 10 kHz, this offset is 0.5, 3, and 6 dB for the PALs at 200, 1000, and 2000 m depth, respectively. There are two consequences for these offsets. Quantitative acoustic measurements of wind speed and rainfall rate depend on the absolute sound intensity at 8 kHz (*Vagle et al.*, 1990) and at 5 kHz (*Ma and Nystuen*, 2005). Secondly, the automatic triggering algorithm for a higher sampling rate was dependent on the absolute sound level, and thus did not trigger as often for the two deeper PALs. Thus, the time step of the acoustic sampling for the two deeper PALs often remains at 5 min (the default), rather than switching to 30 s (the maximum). Fortunately, the signal to noise ratio during rainfall is very high and all instruments usually switched into the high sampling rate during part of each event.

### **3.2. Radar data**

The radar data were collected from the National Observatory of Athens (NOA) high-resolution mobile Doppler dual-polarized X-band (XPOL) radar. It is a low-power (~ 25 kW rms power) radar with selectable pulse and simultaneous transmission of signal at horizontal and vertical polarization. The antenna is mounted on the back of a truck with 8 ft radius and has a 0.95° (3 dB) beam

width. During each storm event the radar was in the Planar Position Indicator (PPI) scan mode at low elevation ( $\sim 2^\circ$ ) above the horizon. The pulse repetition frequency was 1000 Hz with 150 m gate length (range resolution) and 400 gates to give a total range of 60 km. Thus, the nominal backscattering volume at the range of the mooring is 150 m range by 300 m azimuth at an elevation of roughly 500 m above the ocean surface. The scanning rate was less than one minute. The radar was manually operated during storm events, and did not provide continuous temporal coverage. Parts of storm events were missed, but several storms had long periods (several hours) of continuous coverage.

### **3.3. Ground validation network**

XPOL validation is based on the dense network of rain gauges (typical tipping bucket) and a 2D-video disdrometer (2DVD) deployed within a 1-km<sup>2</sup> area and roughly 10 km away from XPOL (see Fig. 1). The gauge network consists of six dual-gauge clusters and a site consisting of three gauges and the 2DVD. Summary of the measured events is presented in Table 1. These data are used to correct the radar rainfall rate estimate for bias during each rain event.

### **3.4. Methoni weather station**

There is a weather station at Methoni that reports wind speed and direction hourly, and rainfall amounts. These data are available during local working hours (0500–1800 LT). This location is 17 km east of the mooring site. There was a bias associated with wind direction when compared to the acoustic wind speed measurements at the mooring. When the winds were from the east, the Methoni wind speeds were consistently lower than the acoustic wind speed measurements at the mooring location (17 km west). When the winds were from the west or northwest, the Methoni wind measurements were closer to the acoustic wind speed measurements (Fig. 5). Acoustic wind speed measurements are typically  $\pm 0.5$  m/s when compared to co-located surface-mounted anemometers (*Vagle et al.*, 1990; *Nystuen et al.*, 2000; *Nystuen*, 2007), and thus this discrepancy is likely to have an orographic explanation.

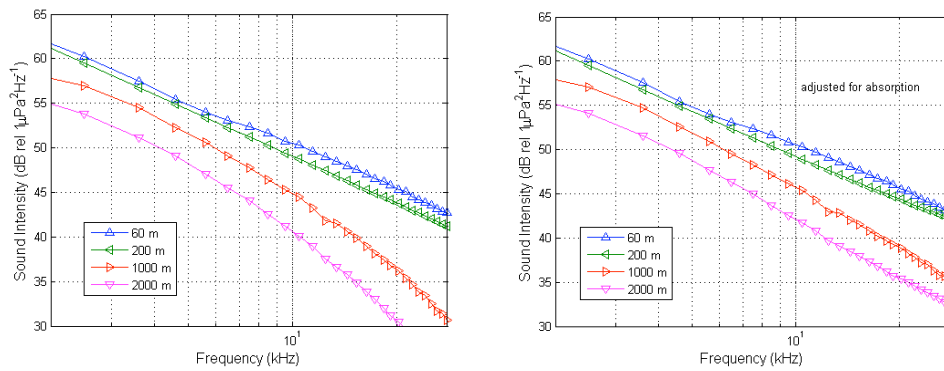


**Figure 4. Mean sound levels at 8-m/s wind conditions. Except for absorption, these spectra should be uniform, indicating a depth-dependent sensitivity correction for these instruments. This change was confirmed in post-experiment testing.**

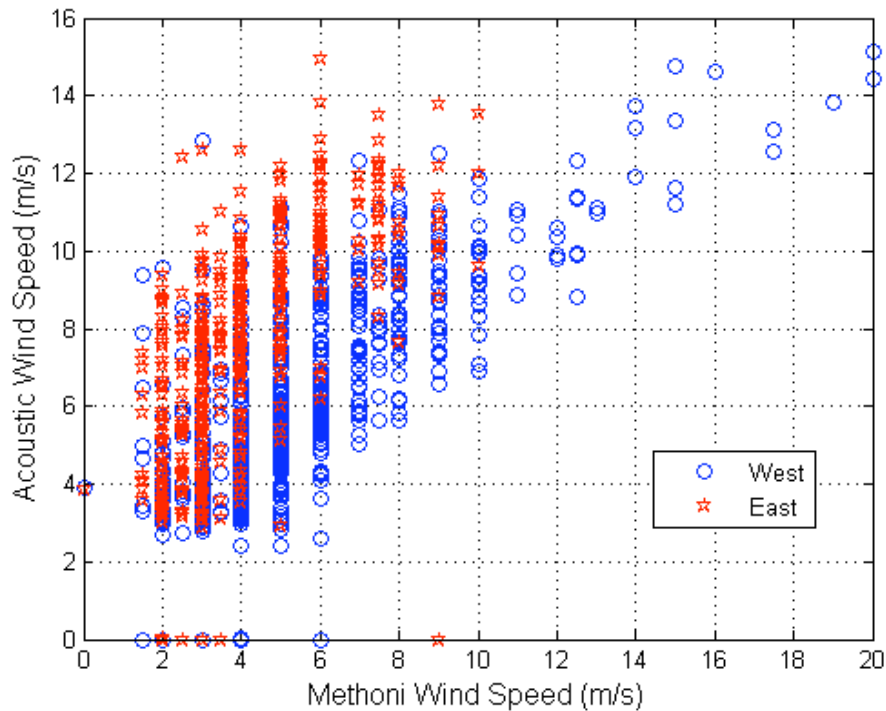


**Figure 5. Comparison of hourly wind speed measurement from the Methoni weather station, recorded manually during daylight hours, and the PAL at 200 m depth (17 km to the west). There is a large bias when the winds are from the east.**

## 4. Acoustic data analysis

Ambient sound in the ocean is a combination of natural and anthropogenic sounds. Various physical processes including wind, rain, and drizzle are primary sound sources in the frequency range from a few hundred Hertz to 50 kHz. These are sound sources at the sea surface. The microphysics of the sound generation are resonating bubbles created during the splashing of wind waves or raindrop splashes (*Medwin and Beaky*, 1989; *Medwin et al.*, 1992; *Nystuen*, 2001). These bubbles are very near the free surface of the ocean, and consequently are assumed to behave as vertically oriented acoustic dipole sources. Human generated sounds include ships and sonars, and different marine animals, especially cetaceans, produce sound underwater in this same frequency band. These human and biological sources should be considered point sources, which may or may not be near the ocean surface depending on frequency, and thus the acoustic directivity of source should not be assumed. An underwater acoustic recorder will hear all of these sounds. Acoustic monitoring requires that the sound be recorded, the source identified and then quantified.

Figure 6 shows a typical three-day record of integrated sound level from the Ionian Sea mooring. The signal from each PAL is overlaid on one another, showing that the signal is present at all recording depths (60 – 2000 m), and is very similar at each depth. The general character of ocean ambient sound is a slowly varying background interrupted by shorter time scale sound events. The slowly varying background sound level can be interpreted as wind speed (*Vagle et al.*, 1990). This interpretation is shown in Fig. 7. Short loud events are mostly ship passages. Longer duration events include rainstorms, including one at 21.8–21.95.

Different sound sources are identified by their spectral characteristics. Features of sound source spectra that can be used to identify the source include spectral levels at various frequencies, ratios of these levels, spectral slopes, and the temporal persistence of the sound source. The data were examined to find times when the sound source could be confidently assumed. Long periods (hours) of steady uniform sound were assumed to be periods of constant wind. Short loud events consistent with typical ship spectra (very loud at low frequency) during non-rainy periods were assumed to be ships. Distinctive rain and drizzle spectra were identified and confirmed with radar. These “typical” sound sources were used to build an acoustic classification algorithm that can be used to objectively identify the sound source in remaining data. The goal is to reliably detect the sound source so that subsequent analysis is not ‘contaminated’ by sound generated by



the source. Figure 8 shows the relationship between 8 kHz and 20 kHz for these ‘test case’ sound sources. This comparison of sound levels at two frequencies is particularly illustrative for demonstrating the ability to use ambient sound to identify the sound sources. Note that there is an ambiguity for the sound source ‘wind = 12 m/s’ and ‘ships’. Other features of the sound field are needed to separate these two sources. For example, periods of high wind are usually of long durations (hours), while ships pass the mooring in minutes. And there may be other spectral measures that are diagnostic. Other useful measures are the sound levels at 2 kHz, the ratio of sound levels from 1 to 2 kHz, the slope of the spectrum from 2 to 8 kHz, the slope of the spectrum from 8 to 15 kHz, and the sound level at 20 kHz.

These relationships change as a function of depth because of absorption (Fig. 9). Since the relationships are used to identify the sound sources, a correction for absorption needs to be applied. Figure 10 shows the scatter diagrams as a function of depth after this correction. For uniform surface sound sources, such as wind, the loci are now independent of depth. For non-uniform sound sources, such as a ship, relatively less low-frequency sound is present at depth, and the position of the non-uniform changes. The classification of loud ships at depth is more difficult as their spectra begins to sound like heavy rainfall.

A sound budget for a location describes the sound levels, sound sources, which sound source is dominant, and the relative loudness of the sources. Different distinctive sound sources are objectively detected based on the spectral and temporal characteristics for that sound source. Exact identity of all sounds in the ocean will never be achieved, however several categories of sounds can be identified. Distinctive spectra for rain (*Nystuen*, 2001) and wind (*Vagle et al.*, 1990) have been described. Different marine animals produce distinctive sounds and can be identified acoustically. Ships and other human sounds are often distinctive, and quite variable.

In the Ionian Sea, objective analysis for five distinctive sounds was attempted: wind, rain, drizzle, shipping, and a 30-kHz clicking that is consistent with the echo location click of cetaceans. The median sound spectrum for each of these sound categories is shown in Fig. 11 for two different listening depths. Note that the signal from shipping is relatively weaker at 1000 m than at 60 m. This may be due to a weaker signal from a point source (ship) than from a uniform surface source (wind or rain). The 30-kHz click signal is actually of similar strength at each depth, suggesting that this source is local, e.g., a whale echo-locating at depth near the PAL. After applying an objective classification code to the data from each listening depth, the sound source can be identified. An example from 3

March is shown in Fig. 12. Once the sound source is identified, different statistics relating to each sound source can be quantified. Table 2 quantifies the percentage of time that each sound source is dominant for four 20-day periods during the deployment. Rainfall is present roughly 6% of the time during the first 20-day period and then is detected 4% of the time during the rest of the experiment. There are also some depth dependent trends. The highest rate for rainfall detection is from the PAL at 200 m, and the lowest is at 2000 m. This may be due to the threshold triggering problem encountered at the deep PALs or because the high-frequency component of the rainfall signal has been attenuated by absorption.

A trend of increasing shipping is evident: from roughly 11% in late January/early February (days 20–40) to nearly 30% of the time in late March/ early April (days 80–100). The shallowest PAL has the highest rate of shipping detection. The shipping signal is dominant at low frequency and distant propagation in the weak sound channel near the surface may allow the shallow PAL to detect ‘distant shipping’ more often than the deep hydrophones. The distant shipping detection often occurs during very calm ocean surface conditions. These conditions increased in duration as the experiment progressed and thus the trend of increasing shipping may reflect an increase in calm ocean conditions as winter changes to summer.

An interesting signal that is present in the data are 30-kHz clicks. The spectral shape of the clicks is shown in Fig. 11 and is consistent with the clicking from beaked whales (*Johnson et al.*, 2004). Beaked whales are a type of cetacean that are difficult to observe visually as they are pelagic and spend a majority of time underwater. It is also a whale type that is sensitive to human noise (*Cox et al.*, 2006). Different cetaceans also echo-locate, but generally at different frequencies, allowing potential identification of the whale type based on the character of the click.

Another clue that these clicks may be from beaked whales is the time and depth pattern of the clicking. Figure 13 shows the time and depth pattern of clicking observed at the mooring. The depth with the greatest number of clicks detected was 200 m. *Johnson et al.* (2004) report that tagged beaked whales began clicking at 200 m depth and dove to a maximum depth of 1267 m. In this situation, clicks are detected at 1000 m regularly, and occasionally at 2000 m. The signal strength is independent of depth, suggesting that the whale is at depth. But clicks are detected at 60 m, which is above the 200 m depth documented by *Johnson et al.* (2004). However, the PALs are listening for a signal; they are not physically on the whale.

**Table 2. Percentage of time that a specific sound source is detected. The deployment is broken into four time periods (days 20–40, 40–60, 60–80, and 80–100).**

<b>Days 20–40</b>	<b>Wind</b>	<b>Rain</b>	<b>Ships</b>	<b>30 kHz click</b>
M – 60 m	81.5	5.8	11.1	0.9
N – 200 m	82.5	7.1	9.1	1.3
O – 1000 m	83.1	4.5	11.8	0.7
P – 2000 m	84.0	2.6	13.4	.07
<b>Days 40–60</b>	<b>Wind</b>	<b>Rain</b>	<b>Ships</b>	<b>30 kHz click</b>
M – 60 m	75.1	2.9	19.6	1.3
N – 200 m	78.1	4.3	15.4	2.1
O – 1000 m	80.4	2.3	16.3	1.0
P – 2000 m	83.2	1.0	15.7	0.1
<b>Days 60–80</b>	<b>Wind</b>	<b>Rain</b>	<b>Ships</b>	<b>30 kHz click</b>
M – 60 m	67.2	3.1	28.7	0.9
N – 200 m	73.5	3.9	21.0	1.6
O – 1000 m	73.2	3.9	22.3	0.7
P – 2000 m	78.3	2.5	19.1	0.1
<b>Days 80–100</b>	<b>Wind</b>	<b>Rain</b>	<b>Ships</b>	<b>30 kHz click</b>
M – 60 m	58.4	3.0	37.9	0.7
N – 200 m	71.0	4.3	23.6	1.1
O – 1000 m	70.0	3.7	26.1	0.3
P – 2000 m	76.2	2.2	21.5	0.05

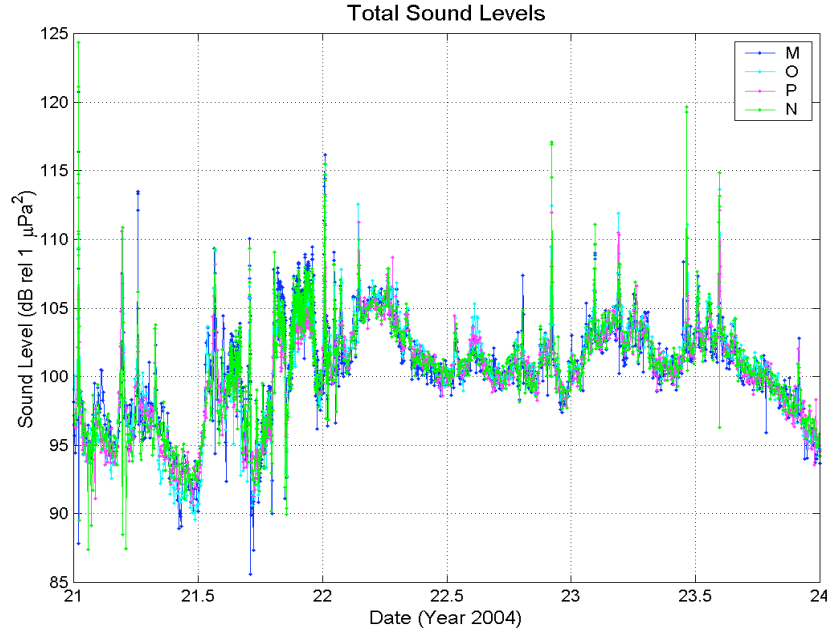


**Figure 6. Total sound levels from 21–24 January 2004. The PALs are at 60, 200, 1000, and 2000 m depth. Short sound events are mostly ships. A rainstorm is present at 21.7–22.0.**

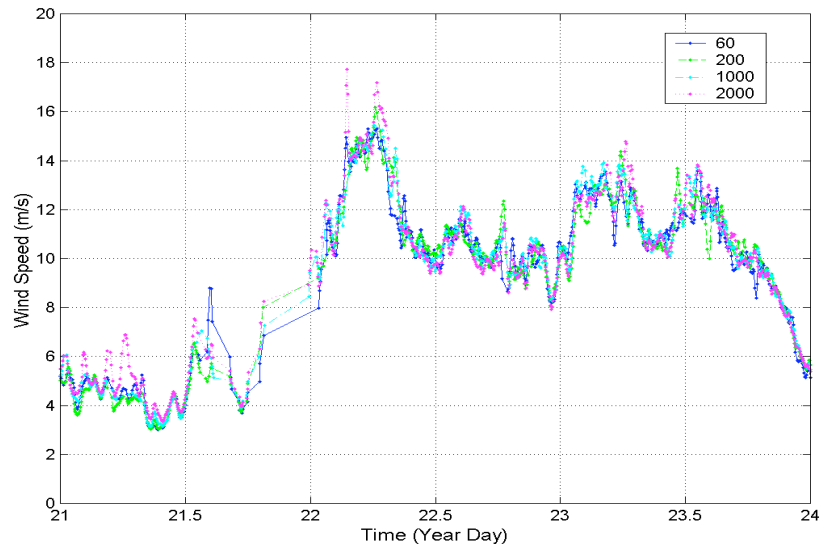


**Figure 7. Geophysical interpretation of the sound field – PAL wind speeds from 21–24 January. Periods when other noise sources dominate the sound field are not interpreted as wind.**

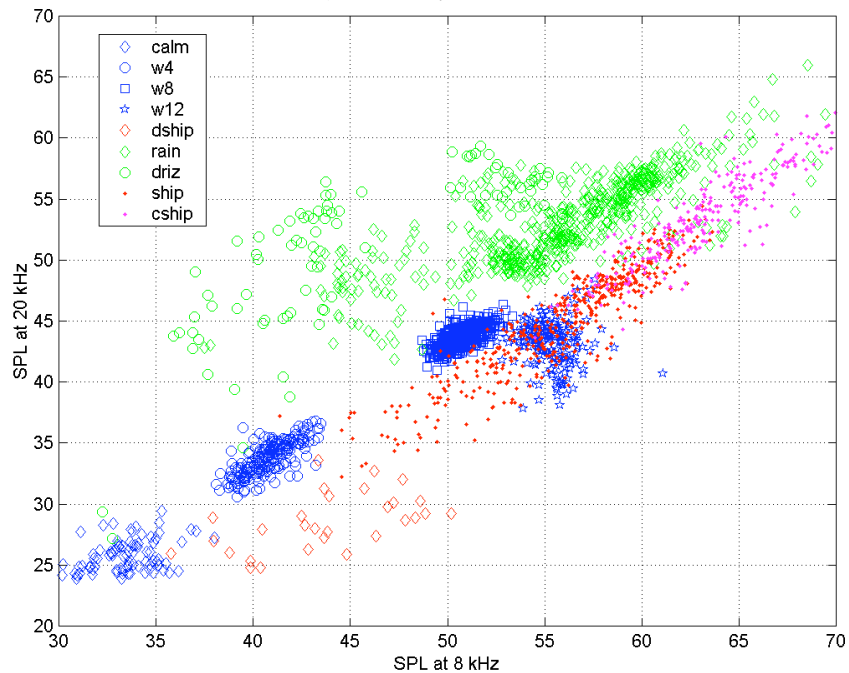


**Figure 8. Scatter diagram showing the ratio of sound levels at 8 and 20 kHz for the PAL at 200 m depth. Different loci of points are associated with different sound sources.**

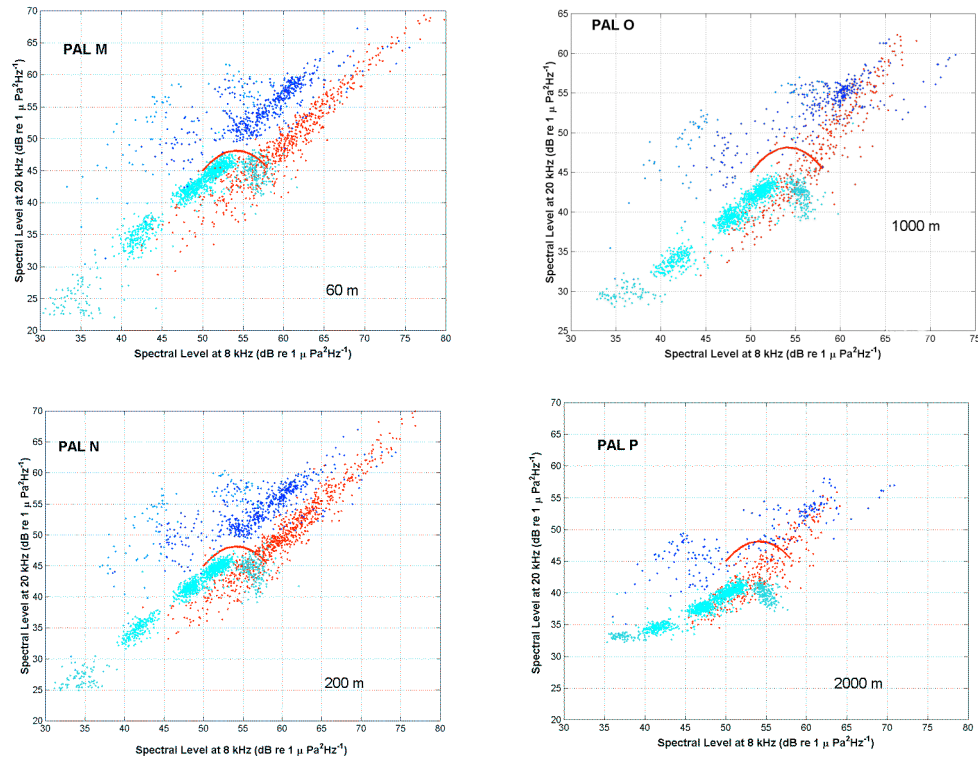


**Figure 9. Scatter diagrams as a function of depth (60, 200, 1000, and 2000 m). Wind (light blue), rain (dark blue), and ship (red) sound sources are shown. The solid curve is at the same location on each sub-figure. Absorption is greater at higher frequencies.**

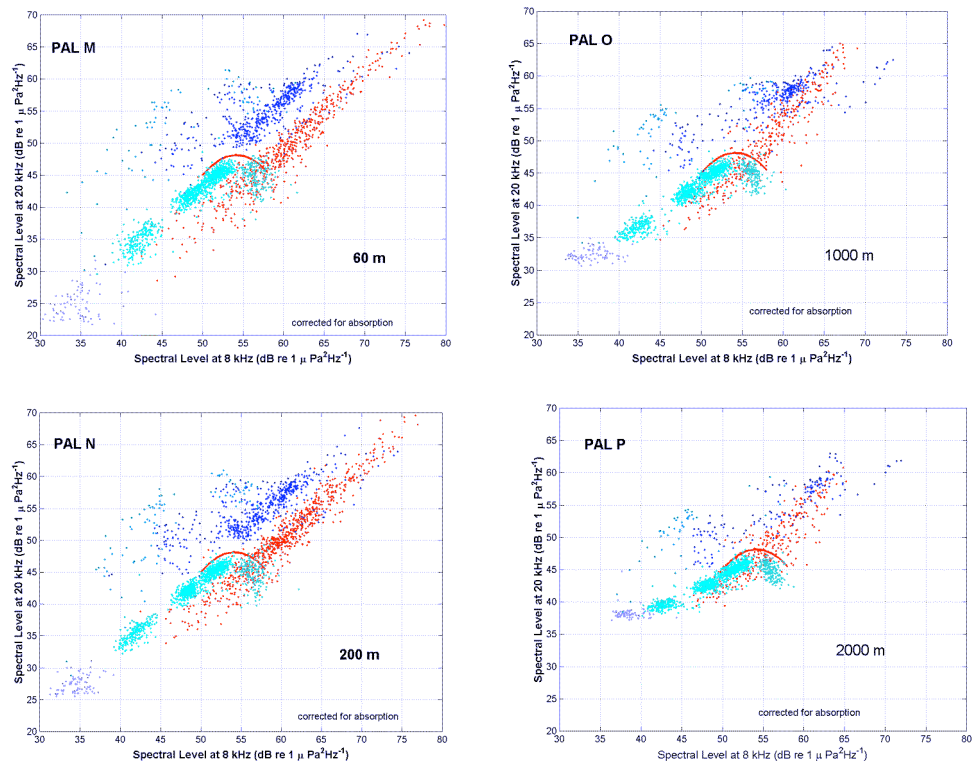


**Figure 10. Scatter diagrams after correcting for absorption. For sound sources satisfying the assumption of uniform sound source, the loci are independent of depth.**

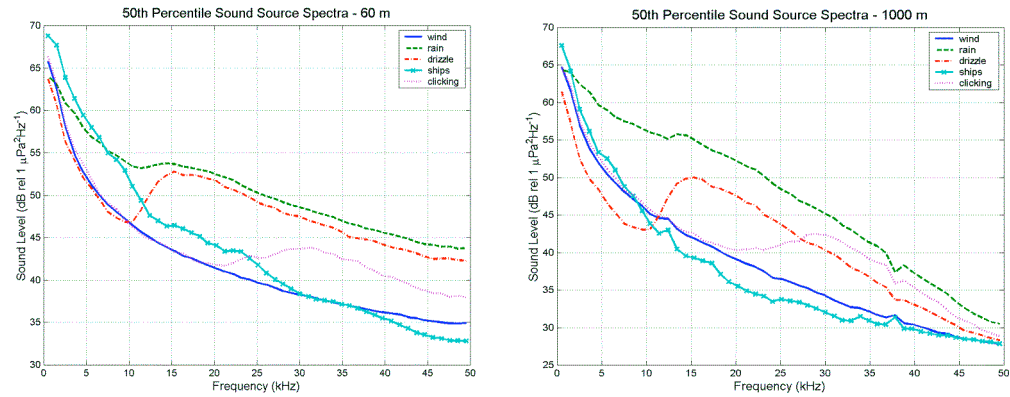


**Figure 11. Spectral signatures of five distinctive sound sources: wind, rain, drizzle, ships, and 30-kHz clicking recorded at the Ionian Sea mooring.**

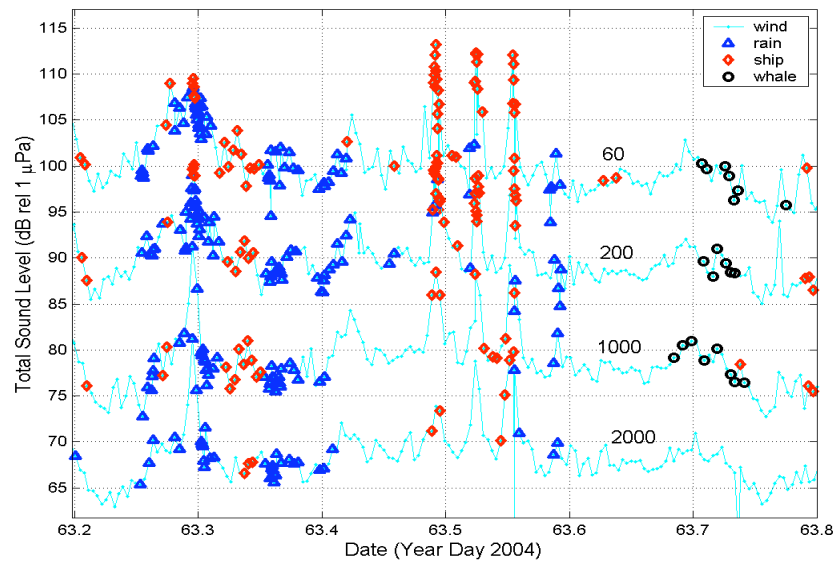


**Figure 12. Integrated sound level at 60, 200, 1000, and 2000 m from Day 63 (3 March). The signals from 200, 1000, and 2000 m are offset by 10, 20, and 30 dB, respectively, for clarity.**

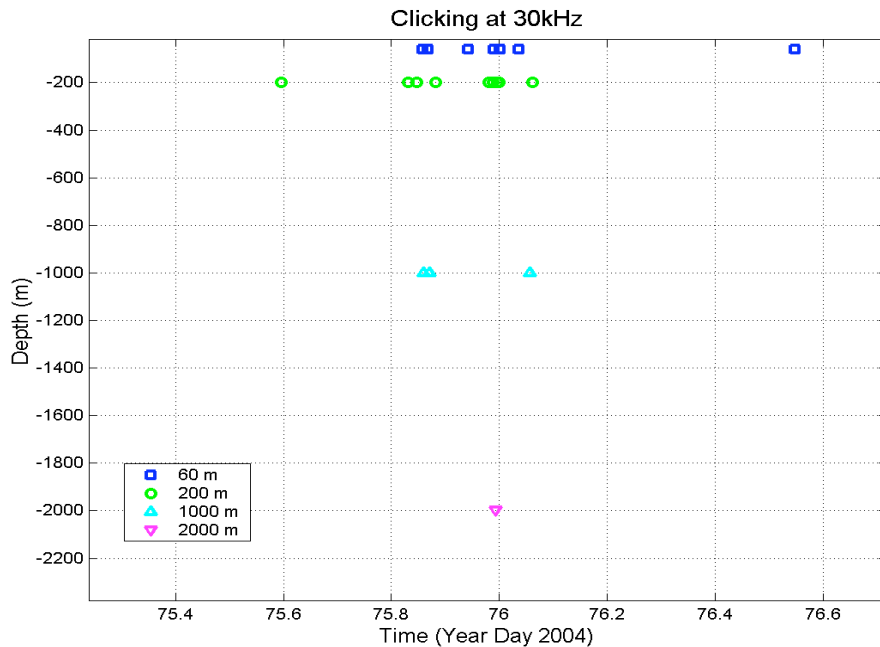


**Figure 13. 30-kHz click detection as function of time and depth. Each symbol indicates a 30-kHz click detection by a PAL. The PALs are located at 60, 200, 1000, and 2000 m depths.**

## 5. Validation of rainfall detection

Validation of acoustic rainfall detection using the radar was available for six rain events: 12 February and 3, 4, 8, 9, and 12 March. The radar was not operating on 21 and 22 January and 1 April. The 12 February event was a complicated frontal weather system within imbedded rain cells and lulls, periods of low winds, high winds, and a few ship passages. On 3 and 4 March were widespread light rain events with low winds ( $< 5$  m/s). March 8 was a day with high winds ( $\sim 10$  m/s) and included an isolated squall line. March 9 and 12 were both relatively long, continuous rain events in moderate (5–10 m/s) wind conditions. Radar coverage was not complete on 12 February and 3 and 8 March.

### 5.1. Case Study – 12 February 2004

On 12 February 2004 a frontal system passed over the mooring. This was a complicated system consisting of several rain cells and lulls. The acoustic record of the day contains a wide variety of signals, including distant shipping, a close ship passage, some loud noises, and the sound of high wind conditions. An acoustic overview of the day is shown in Fig. 14, with the periods when different acoustic signals were recorded labeled and described in Table 3. The XPOL radar data are also shown on this figure with three different thresholds: over 1 mm/hr, over 2 mm/hr, and over 5 mm/hr. The radar was not turned on until Min 240, missing the initial rain events (periods B and D). Period E shows the strongest radar rainfall, with light rain detected in Period H. Period I is apparently a strong but brief rain cell. The radar was turned off at Min 1080, after the passage of the weather front.

Sound spectra for each time period are shown in Fig. 15, and the classification diagrams are shown in Fig. 16. The start of the day (Period A) shows the typical spectra of the sound category ‘distant shipping’. In this situation propagation conditions are excellent and distant low-frequency (under 2 kHz) sound is detected, but the sound levels at high frequency (over 20 kHz) are very low, suggesting that the high-frequency sound from the distant source has been absorbed. The ocean surface is very flat (no wind waves), allowing good reflectivity for order decimeter wavelength sound waves from the surface. This signal ends as the first light rainfall occurs (Period B), likely ruffling the surface and reducing long range propagation of the low-frequency sound. Note that the sound levels below 10 kHz actually drop between Periods A and B, although there is likely more local sound being generated in Period B. At high frequency the sound levels in Period B are elevated by bubbles from small raindrop splashes. A ship passes at Min 180 (Event C), producing a ‘typical’ ship spectrum with very high sound levels below 2 kHz, and a consequently relatively steep spectral slope



between 5 and 15 kHz. In contrast, rainfall produces a relatively flat spectral slope between 5 and 15 kHz.

The first strong rain cell occurs in Period D. This cell is detected by all four PALs and has high sound levels at all frequencies, but especially between 2 and 20 kHz where larger raindrops produce sound from their splashes. This signal often obscures the 13–25-kHz signal from small raindrops, as is apparently the case in this example. In contrast, Period E is a longer, more continuous rain, with a few stronger rain cells imbedded in a non-homogeneous rain field. The XPOL weather radar was turned on at Min 240, was offline from 265–285 and then on again after Min 285, verifying rainfall over the mooring. Period E will be described in more detail below. Within Period E, a loud sound was detected at Min 373. This spectrum is shown in Fig. 15, and the classification points in Fig. 16 put it into the category of ‘a close ship passage’, however the peak in this spectrum at 4 kHz is not a ‘typical’ ship signature. Sometimes ship engines ‘howl’, and this may be the case here. There is no strong radar echo at Min 373, and so it is not rainfall.

Period G is an interlude between rain events. The winds are low, under 5 m/s, and rise gradually during this period. A typical wind spectrum is recorded by all four PALs, and no rain conditions are verified by the radar. The radar reports light rainfall during Period H. During this time period there is partial acoustic detection of rainfall (see Fig. 16) with relatively high sound levels at lower frequencies, suggesting that the wind speed is relatively high (~8–10 m/s). At Min 800, the wind speed increases to over 10 m/s and becomes steady for many hours. The Methoni weather station reported sustained winds over 15 m/s. The sound levels above 20 kHz actually drop, and are relatively lower than the sound levels when the wind speed is less (Period G). This is due to ambient bubble clouds below the ocean surface from breaking waves. These small bubbles are absorbing the high-frequency sound being produced at the ocean surface by newly breaking waves, and thus distort the spectral sound signature of those waves. [Wind speed is measured using the sound level at 8 kHz (*Vagle et al.*, 1990) to avoid this distortion of the signal from absorption. Bubbles that absorb sound at 8 kHz are large enough that they rise to the surface quickly.]

The longest sustained rain event (Period E) is examined in more detail in Figs. 17 and 18. Figure 17 shows the acoustic detection and classification for all four PALs, at depths 60, 200, 1000 and 2000 m, while Fig. 18 shows the time series of the sound levels with the classifications of rain and shipping shown. The acoustic rainfall signals are overlaid on one another and show that the rainfall signal is similar at all depths. Distinct periods during this period are again labeled (1–20),

plus there is a ship detection between Periods 10 and 11 that will be referred to as Event A. The radar data is shown at +200 m (an arbitrary height) for a rainfall rate threshold above 1 mm/hr. The radar was not operational before Min 240, missing the initial strong rain, labeled Periods 1–5 in Fig. 17. The radar was also “off line” during Period 7. Table 4 presents the acoustic and radar interpretation for each identified period. The strongest radar reflectivities are at Periods 9 and 12. Light rain is detected by the radar at Periods 6, 17, and 19. The mean spectrum for the lulls (Periods 1, 5, 13, 16, 17, and 18) is the typical spectrum for 6-m/s wind conditions, suggesting that the background wind is about 6 m/s. The Methoni weather station reports 4 m/s during this part of the day. The acoustic wind measurement is 4 m/s at Period 20. The two ship detections are verified by the absence of radar rainfall detection at Min 343 and at Min 373. There was rain detected at Mins 375–380, however the acoustic signal at Min 373 (Signal F in Fig. 15) is very loud and would require a rainfall rate over 100 mm/hr if it were classified as rain. Note that the ship at Min 343 is not well detected at depth (Fig. 17). In fact, it is not detected by the deepest PAL. The signal from a ship is a point source, in contrast to a wide-spread surface source from rain, and is relatively weaker at depth. The ship detection at Min 343 may be a more distant ship, with sound propagating near the surface. The ‘loud sound’ at Mins 373–375 (Signal F in Fig. 15; Period 14) is detected by all of the PALs and is presumably a ship passing very close to the mooring.

Once classification is established, a comparison of rainfall rates is possible. Fig. 19 shows the comparison of the shallow PALs, at 60 and 200 m, with the XPOL radar rainfall rates averaged over a 0.75-km (5 cells) radius circle above the mooring location. Two radar rainfall estimates are presented: one is based on a Z/R relationship for reflectivity to rainfall rate and the second on a ZdR relationship that uses the differential polormetric reflectivity to account for drop distribution variations in the rain. The strong rain cell (PALs) at Min 325 is Period 9 in Fig. 17 and the strong rain cell at Min 355 is Period 12. The correlation coefficients when the radar is operating and the acoustic data are good (no ship contamination present) are roughly 0.8.

## **5.2. Case study: Light rain in light wind conditions – 3 and 4 March**

Light wind conditions are ideal for the sound production mechanism for small raindrops (1 mm diameter) (*Nystuen*, 2001) and that sound is surprisingly loud. This drop size is present in most light rain (< 1 mm/hr) and consequently drizzle is easily detected acoustically during light wind conditions. The co-detection of light rainfall on 3 and 4 March was high, even during intermittent periods of light

rain. Fig. 20 shows the comparison of rainfall rates, quantified after detection, for 3 March. Note that the radar was not operational before Min 432 and thus missed the rain cell at Min 420. The radar rainfall rates were low, and yet all of the times that the radar reported rain are confirmed by acoustic detection.

### **5.3. Case study: Moderate rain in moderate wind conditions – 9 and 12 March**

Both of these events had long periods of rainfall with co-detection by both the radar and the PALs (Fig. 21). On 9 March, shipping contamination is detected from Mins 725–750 at the shallow PALs and these data are discarded from further analysis. This shipping contamination was not well detected at depth (the PALs at 1000 and 2000 m) suggesting that the noise source is an isolated point source, i.e., a ship that is ‘averaged out’ when heard from a distance. On 12 March the rainfall starts as a relatively strong rain (6 mm/hr) (Fig. 22) and then tapers off after Min 910. This is evident in the classification diagrams for 12 March (Fig. 23). The wind speed is relatively high during this event, with acoustic wind speed measurements of ~10 m/s before the start of the event and 8 m/s at the Methoni weather station (17 km to the east). Methoni reports a drop in the wind speed to 6 m/s during the rain; no acoustic wind speed estimates are available during the rain. The PAL rainfall rates have been divided by a factor of two in Fig. 22, suggesting that the quantitative rain signal has been affected by the high wind. On the other hand, detection of rainfall remains excellent (Fig. 23).

### **5.4. Case study: Squall line on 8 March**

Perhaps the most serendipitous rain event was an isolated squall line that passed over the mooring on 8 March. The radar scan for this event is shown in Fig. 24 shortly after the passage of the squall line at the mooring location. Based on the echo-location position of the squall from consecutive radar scans, the local wind speed is 7 m/s. The acoustic wind measurement at the beginning of the squall is 9 m/s, in agreement with the wind measurement at the Methoni weather station. A comparison of rainfall rates is shown in Fig. 25. One comparison of rainfall rates is from the shallow PALs (60 and 200 m) and the XPOL Zdr rainfall rate averaged over a 0.75-km radius circle (5 cells) over the mooring. This shows that the rain cell is short (2–3 min) and intense (60–90 mm/hr). The second comparison is from the deeper PALs (1000 and 2000 m) and the XPOL Zdr rainfall rate averaged over a 4.5-km radius circle (30 cells) over the mooring. The rain cell detection is longer, of order 10 minutes, and less intense (15–40 mm/hr). This is consistent with spatial averaging of an intense small rain cell over a larger area and is evidence of a larger listening area for the deeper hydrophones.

A curious feature of this rain event is a ‘moment of silence’ at Min 909 (Fig. 26). Fig. 26 shows the sound levels at 5 kHz during the passage of the squall line. The PALs are totally independent of one another, and so this is a real feature. Note that the sound level at 200 m is actually quieter than the sound levels before or after the squall line. This suggests that the sound production mechanism for wind (breaking waves) has been disrupted by the intense rain. It is widely reported, but undocumented, that ‘rain calms the seas’. This is acoustical evidence that this is true. The radar reports no echo return at Min 909 (Fig. 25) in the cell directly over the mooring, and the radar scan at Min 915 (Fig. 24) shows an abrupt end to the backside of the squall. Note, however, that severe attenuation of the radar signal through the rain cell may also cause ‘no echo’ return from the radar. The acoustical evidence suggests that this is not the case here.

**Table 3. Time periods with acoustic interpretations for 12 February 2004.**

<b>Period</b>	<b>Acoustic Interpretation</b>	<b>Radar</b>
A	distant shipping	off
B	light drizzle	off
C	ship passage	off
D	rain cell	off
E	steady rain	rain
F	loud noise	no rain
G	wind	no rain
H	light rain	light rain
I	uncertain	rain cell
J	high wind	no rain

**Table 4. Time periods with acoustic and radar interpretations for the major rain event on 12 February 2004. Note that Event A, a ship passage, occurs between Periods 10 and 11.**

<b>Period</b>	<b>Time</b>	<b>Interpretation</b>	<b>Radar</b>
1	200-210	lull	off
2	215-220	rain	off
3	220-223	downpour	off
4	225	rain	off
5	230	lull	off
6	240-265	light rain	light rain
7	265-285	light rain	off
8	285-320	rain	rain
9	325-327	downpour	rain cell
10	345	rain	rain
11	350	rain	rain
12	355-360	downpour	heavy rain
13	360-370	lull	lull
14	373	very loud noise	lull
15	375-380	rain	rain
16	390	lull	lull
17	405	lull	light rain
18	415	lull	lull
19	430	light rain	light rain
20	440	lull	lull
A	339-341	ship	lull

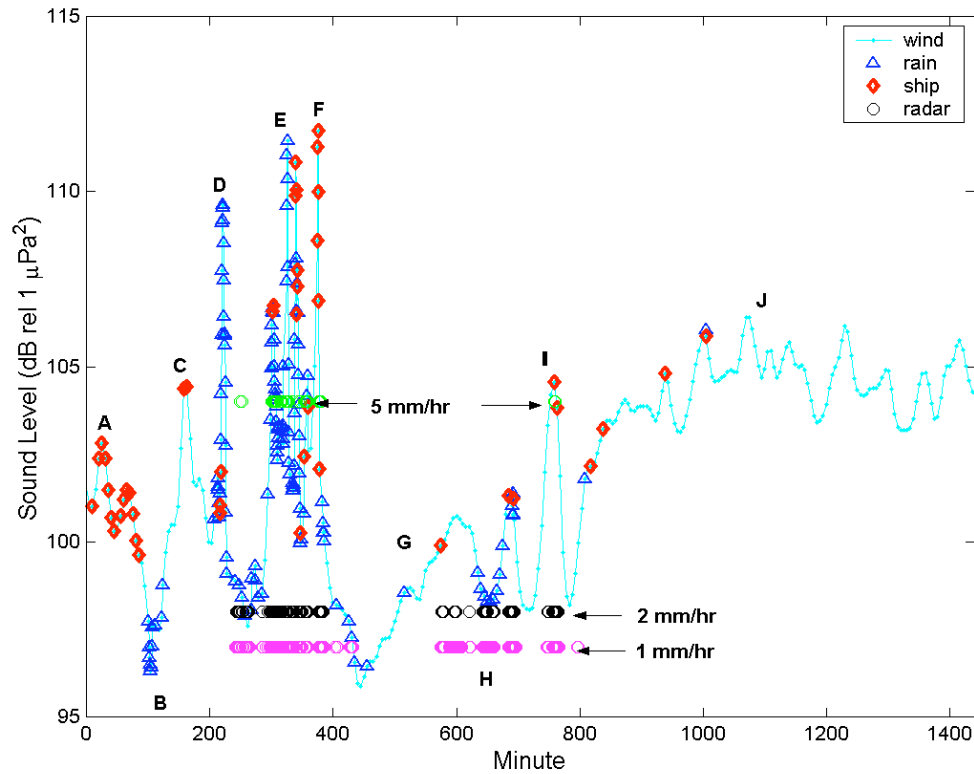
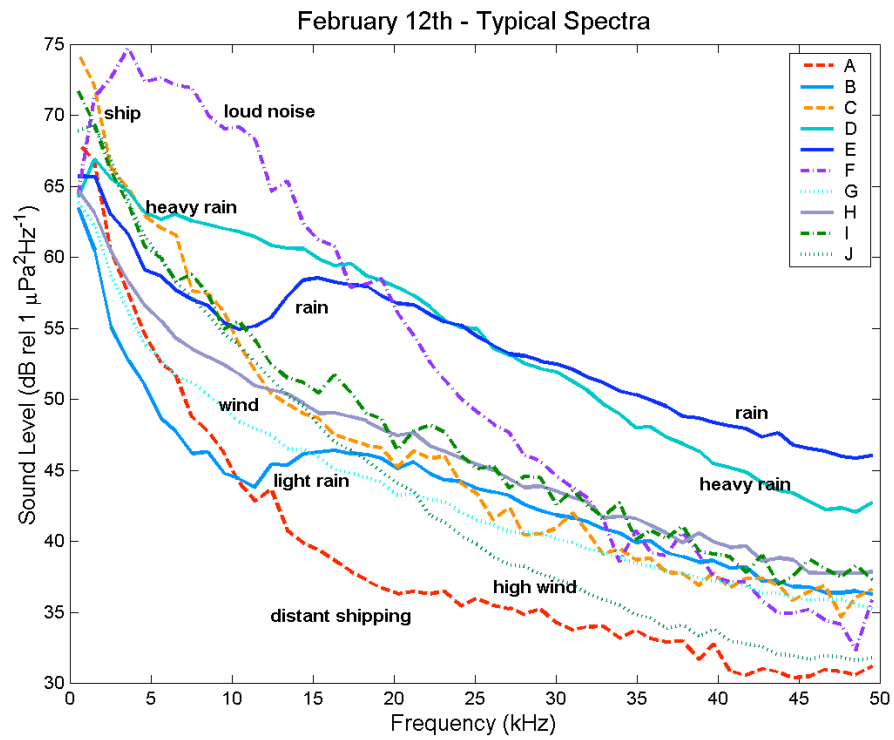
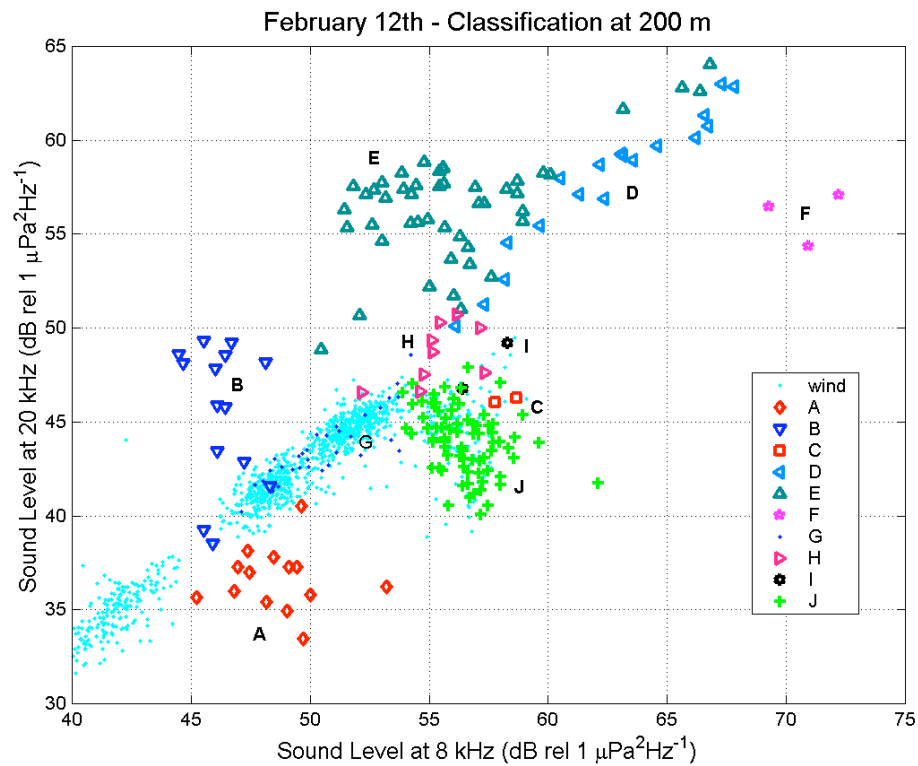


Figure 14. The time series of sound level from PAL N at 200 m depth during 12 February 2004. Distinctive periods of the day are labeled A–J. Rainfall and shipping detections are shown. The XPOL radar rainfall detection is shown at three different thresholds: 1 mm/hr, 2 mm/hr, and 5 mm/hr.



**Figure 15.** Typical sound spectra for different periods of the day on 12 February 2004 from PAL N at 200 m depth.



**Figure 16. Classification diagram for PAL N at 200 m on 12 February 2004. The ‘wind’ points are a background reference for the entire deployment for ‘wind only’ conditions. Deviations from these points are ‘other’ sound sources including rain, drizzle, and shipping.**



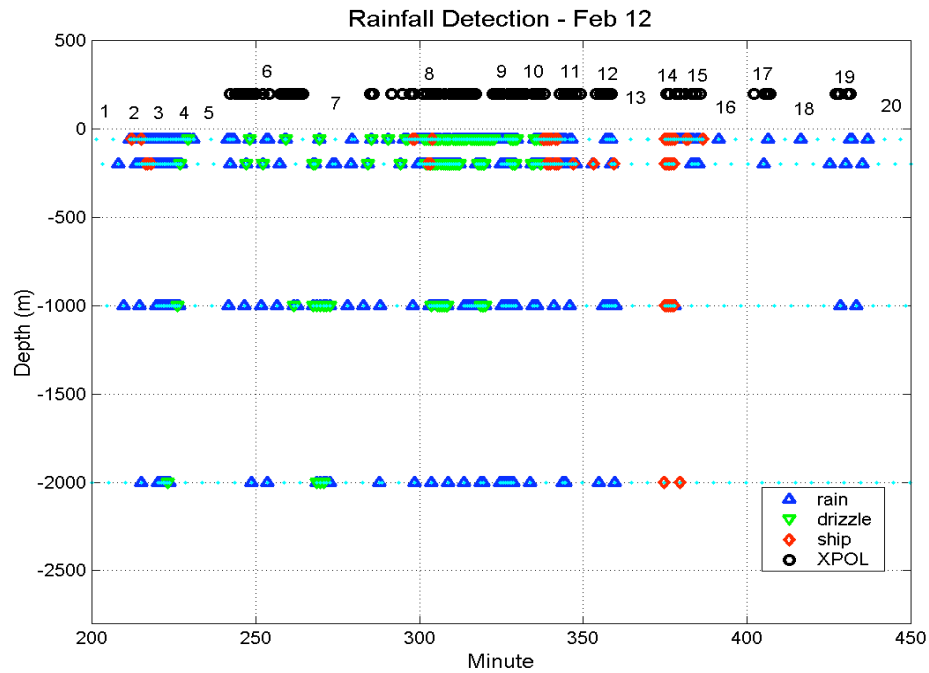


**Figure 17. Detection and classification of rainfall as a function of depth. The detection and classification of the sound source are shown for each PAL at 60, 200, 1000, and 2000 m. The XPOL radar data is shown at +200 m for radar rainfall rates above a 1-mm/hr threshold. The radar was not operating before Min 240 (periods 1–5) or during Period 7.**

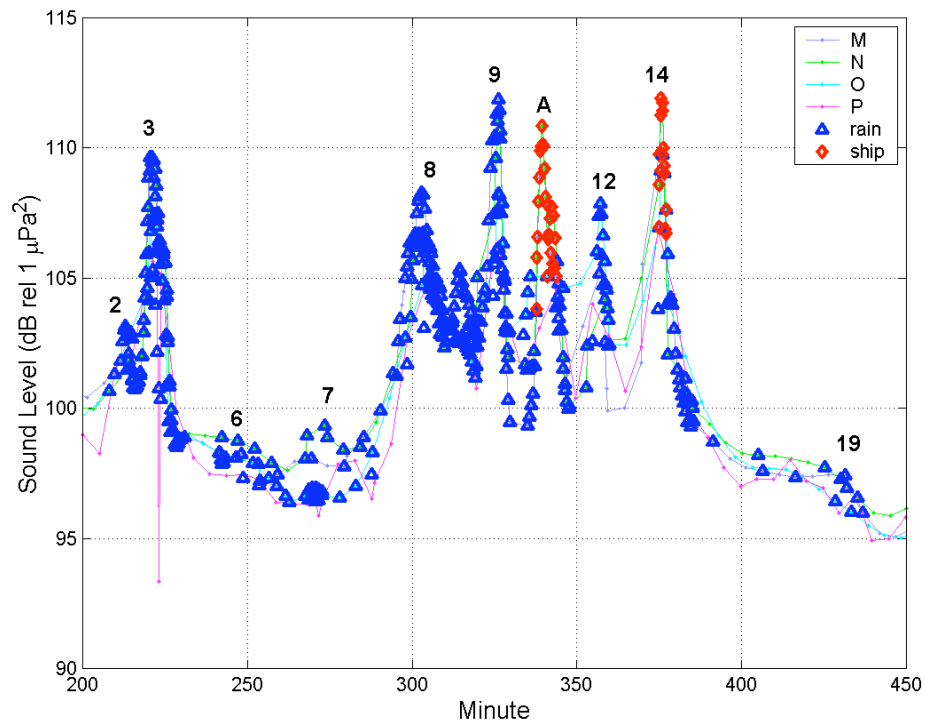


**Figure 18. Time series of sound levels for all four PALs during the main rain event on 12 February 2004. The four time series overlay one another. Classification as rain and ships are shown. Selected labels refer to the time periods shown in Fig. 17 and Table 4.**

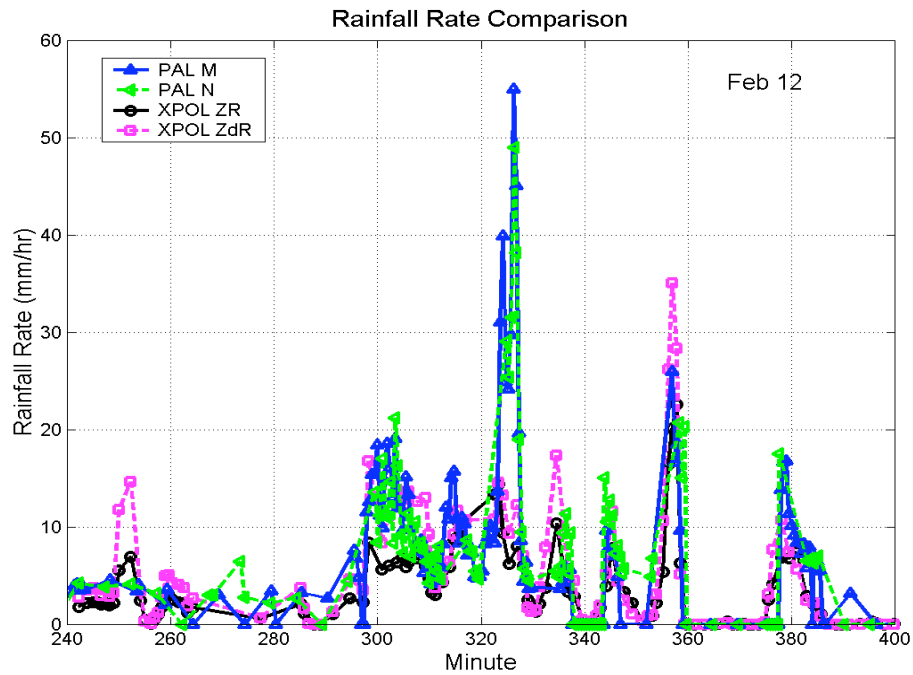


**Figure 19. Rainfall rate comparison between the shallow PALs at 60 and 200 m, and the XPOL Z/R and ZdR rainfall rates averaged over a 0.75-km radius circle centered above the mooring.**

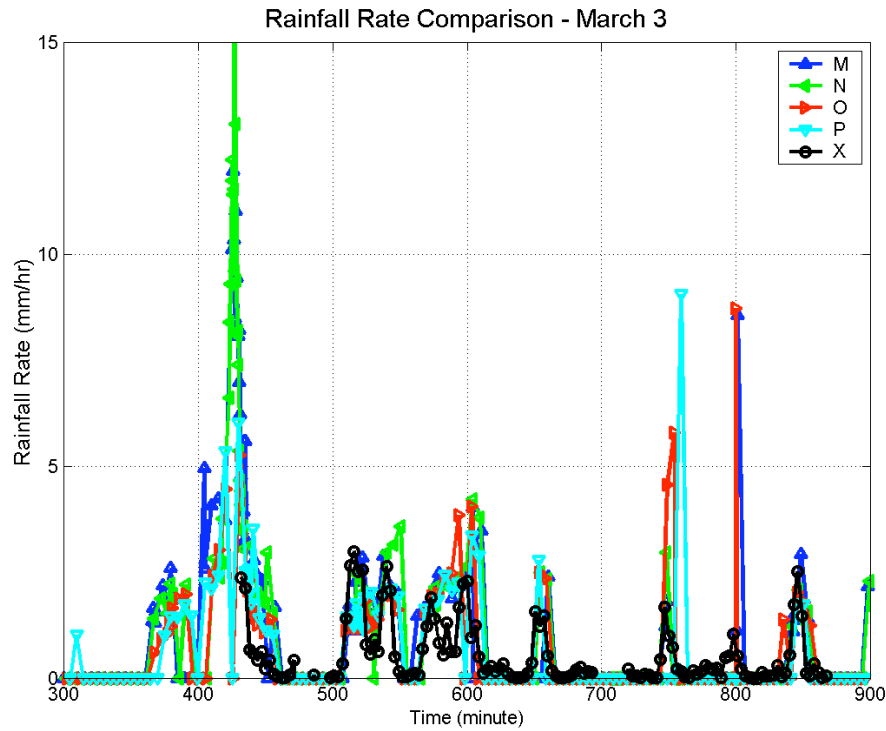


**Figure 20. Comparison of rainfall rates on 3 March. The radar was not operational before Min 432.**

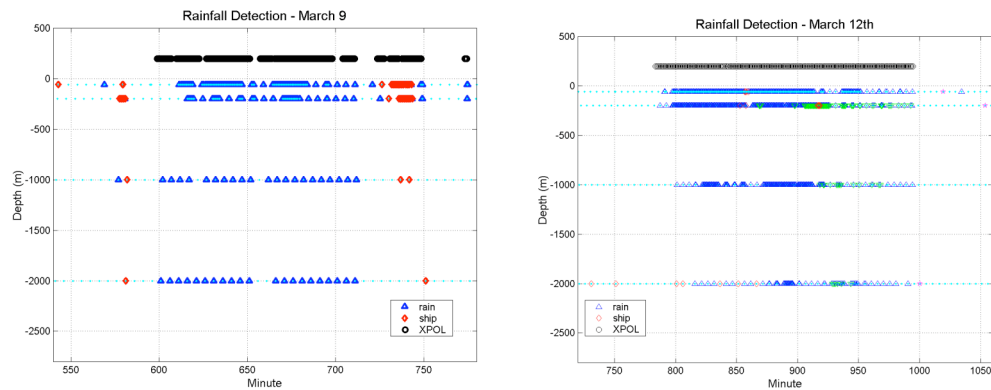


**Figure 21. Rainfall detection validation on 9 and 12 March. The data from each PAL are shown at the depth of the PAL (60, 200, 1000, and 2000 m). The radar rainfall detection is for a threshold of 1 mm/hr and is shown at +200 m elevation. Note the shipping contamination for 9 March at Mins 720–750. Light rain is detected during Mins 920–980 on 12 March.**

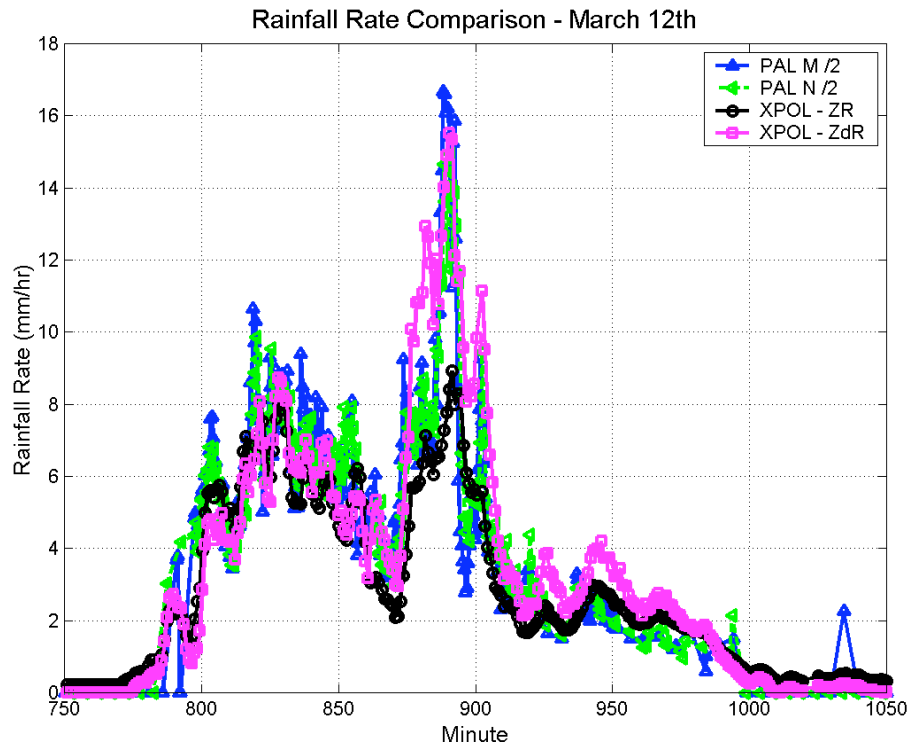


**Figure 22. Comparison of XPOL radar rainfall rates and PAL rainfall rates on 12 March. Two rainfall rate estimates are available from the radar: a Z/R relationship relating reflectivity to rainfall rate and a ZdR relationship using the dual polarization feature of the radar to ‘improve’ the retrieval. The radar data have been averaged over a 0.75-km (5 cells) radius circle above the mooring. The PALs shown here are at 60 and 200 m (the shallow PALs).**

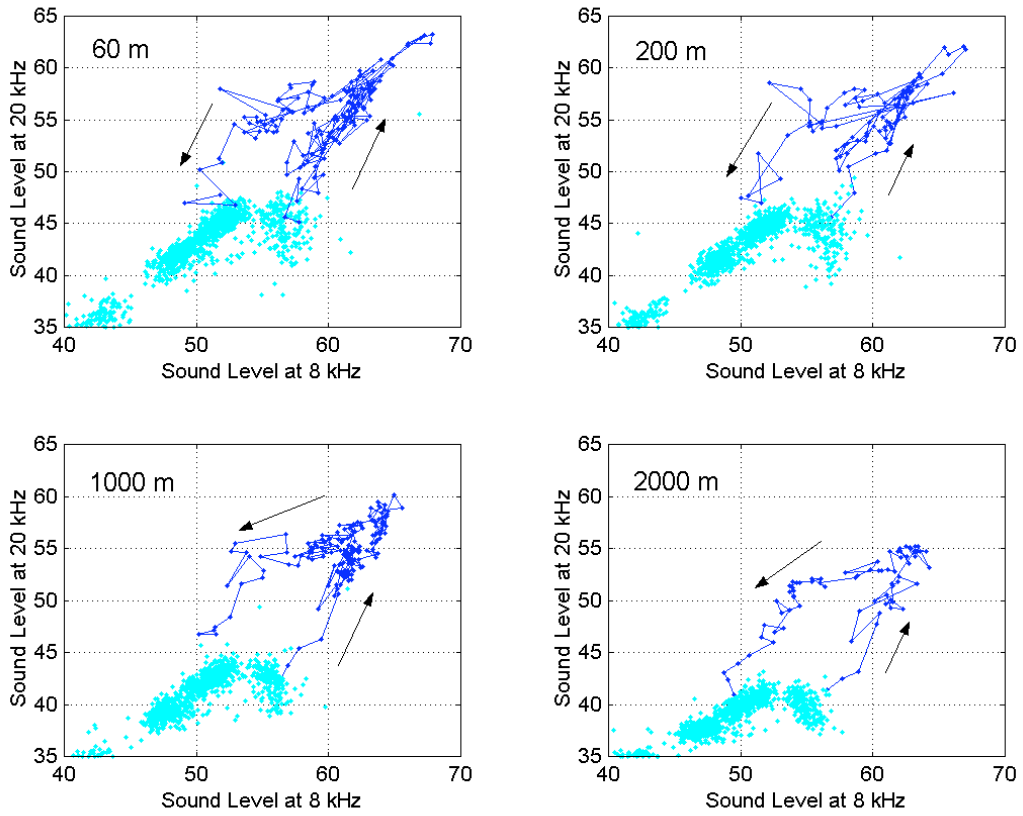


**Figure 23. Classification diagrams for 12 March. The light points are reference ‘wind only’ points. The dark points are during the rainfall event on 12 March. The arrows indicate the advance of time. Initially the rainfall is heavy and then it tapers off into the drizzle classification zone.**

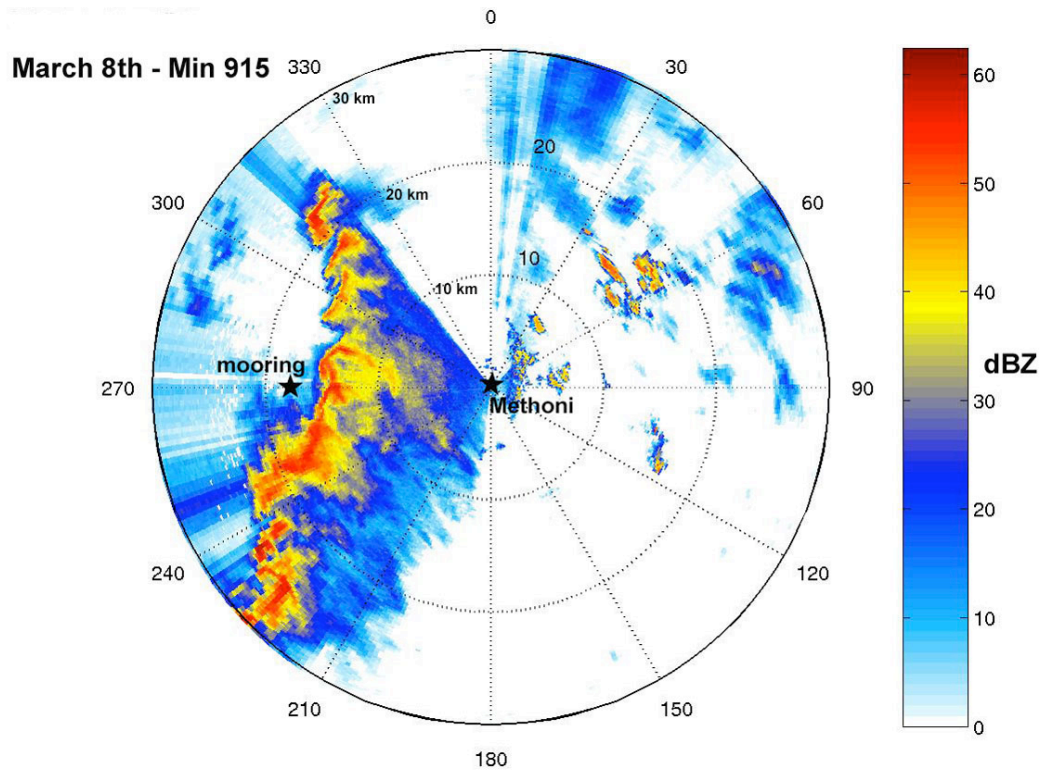


**Figure 24. Radar PPI scan at Min 915 on 8 March. The squall line passed over the mooring from Mins 900 to 905. There was a moment of silence at Min 909. Based on echo-location motion the wind speed is 7 m/s.**

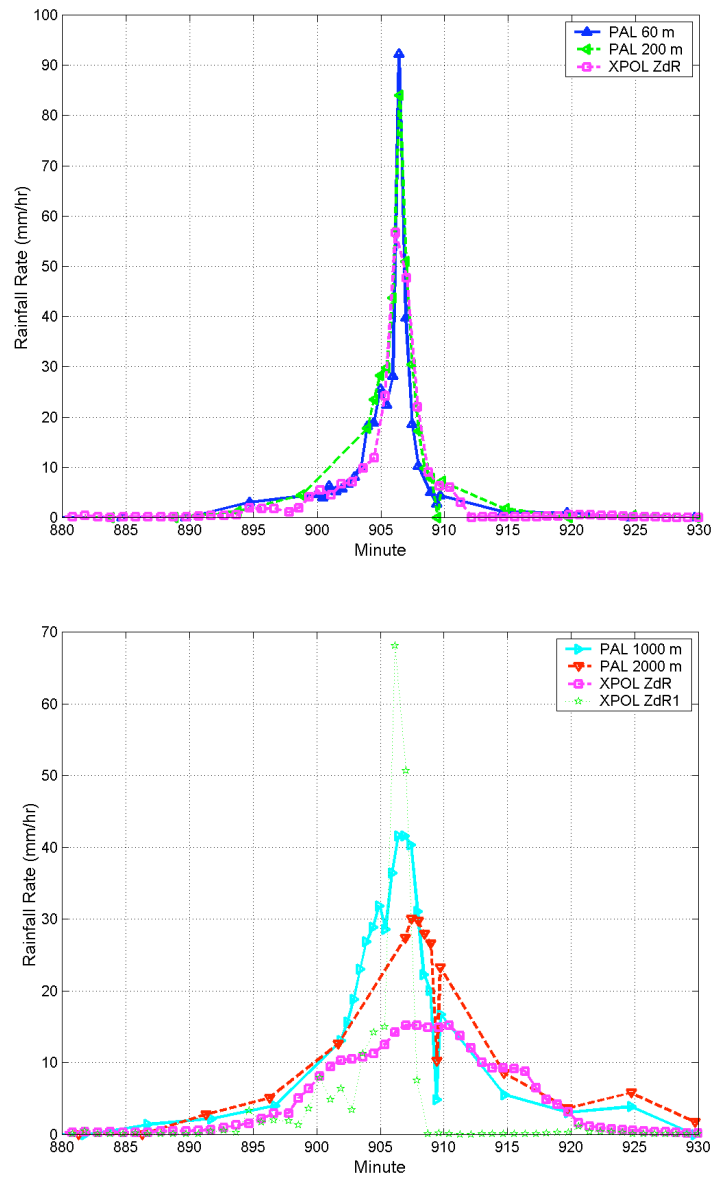


**Figure 25. Comparison of rainfall rates during the squall line on 8 March.** The top panel shows the comparison between the shallow PALs (at 60 and 200 m) and the radar Zdr rainfall rates averaged over a circle of radius 0.75 km (5 cells) centered over the mooring. The bottom panel shows the comparison between the deep PALs (at 1000 and 2000 m) and the radar Zdr rainfall rates averaged over a circle of radius 4.5 km (30 cells) centered over the mooring. This panel also shows the radar rainfall rate at the mooring (single cell) indicating that the rain had completely stopped by Min 909, when a ‘moment of silence’ was recorded.



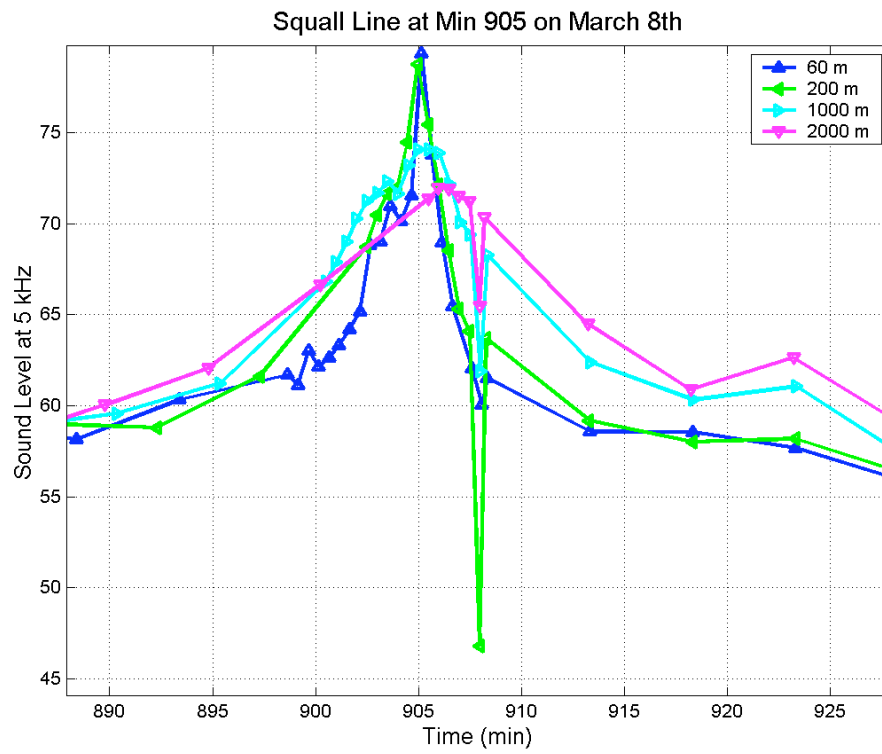


**Figure 26. Sound levels during the passage of the squall line on 8 March. All four PALs detect a drop in sound level at Min 909. The sound level recorded at 200 m is actually lower than the sound level before or after the squall line.**

## 6. Spatial averaging of the rainfall signal

Three examples of coincident observations of relatively continuous rainfall are used to investigate the spatial averaging of the acoustic rainfall signal (12 February and 8 and 12 March). The rainfall rates from the PALs are compared to averaged rainfall rates from the radar for different averaging radii in a circle centered over the mooring location. The results are shown in Fig. 27. The clearest result is for the squall line on 8 March. This event had a much smaller spatial and temporal scale than the other two examples. The averaging radii producing the highest correlation between the radar and the PALs increase from 450, 750, 1500, and 3000 m for the measurements at 60, 200, 1000, and 2000 m, respectively. The prediction assuming a uniform weighting of the acoustic signal within the listening area from Fig. 3 was 170, 610, 2735 and 4800 m, respectively. Thus, the signal from the shallowest hydrophone is most highly correlated to the radar rainfall measurement averaged over a larger listening area than expected, and the deeper hydrophones to smaller areas than expected.

It was noted that the weighting of the acoustic signal is not uniform, but is weighted towards the center of the listening area, thus reducing the expected listening area for the hydrophones. When the other two examples are considered, the averaging radii producing the highest correlation for the PAL at 2000 m remains between 3 and 4 km. This suggests an effective listening area of about  $\pi r^2 = 30\text{--}50 \text{ km}^2$ . In contrast, the averaging radii producing the highest correlation for the PAL at 60 m goes from 450 m for the squall line on 8 March to 1 and 2 km, respectively, for the rain events on 12 February and 12 March. These events were more widespread with longer spatial and temporal time scales, suggesting that physical scale of the rain itself may be responsible for this result. Nevertheless, the trend is as expected. The deeper acoustic measurements have higher correlations to the radar rainfall averaged over larger apparent listening areas. The intermediate PALs at 200 and 1000 m show intermediate results.

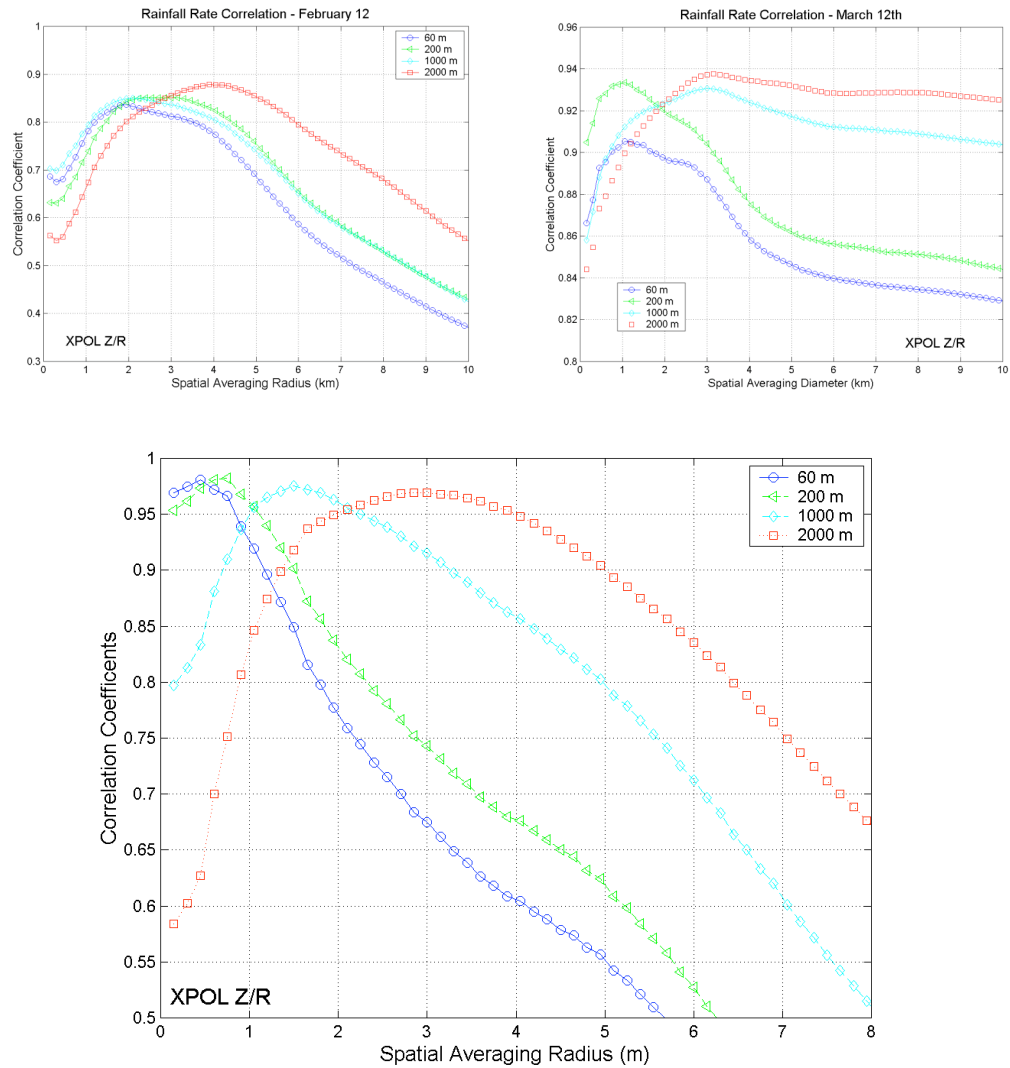


**Figure 27. Correlation coefficients between the acoustic rainfall measurements at 60, 200, 1000 and 2000 m depth compared to the averaged radar rainfall rates averaged over circles of different radii centered over the mooring. The radar cell size is 150 m.**

## 7. Conclusions

High-frequency (1–50 kHz) acoustic measurements of the marine environment at four depths (60, 200, 1000, and 2000 m) are used to describe the physical, biological, and anthropogenic processes present at a deep water mooring site near Methoni, Greece from mid-January to mid-April in 2004. The acoustic signal is classified into five categories: wind, rain, drizzle, shipping, and a 30-kHz clicking that is consistent with deep-diving beaked whales. The background acoustic signal is from breaking wind waves, and is nearly identical at all listening depths. This signal is clean, that is, not contaminated by other sound sources, 70–80% of the time and can be used to quantitatively measure wind speed (*Vagle et al.*, 1990). The accuracy of this measurement is often  $\pm 0.5$  m/s (*Nystuen et al.*, 1998; *Ma and Nystuen*, 2005; *Nystuen*, 2007), however comparisons with the Methoni weather station 17 km to the east show a systematic bias when the winds are from the east or southeast (Fig. 5) during this experiment.

The mooring location is near an ocean shipping lane and consequently frequent close passages of ships were detected acoustically. These events are usually loud at all frequencies (1–50 kHz) and brief (a few minutes) with relatively high low-frequency sound levels allowing their detection and classification at all hydrophone depths. Another category of shipping noise is ‘distant shipping’. Very calm ocean surface conditions allow the propagation of distant shipping sound near the ocean surface, especially at lower frequencies ( $< 2$  kHz) where the shipping signal is often relatively loud and sound absorption by seawater is relatively low. In contrast, higher frequency sound ( $> 10$  kHz) is absorbed and does not propagate long distances (tens of kilometers). These conditions were more prevalent in the later periods of the experiment and the level of ‘shipping’ acoustically detected increased significantly from 12% of the time in the first part of the experiment to over 25% of the time at the end (Table 2). This increase was most pronounced at the shallowest hydrophone at 60 m depth. This depth was within a weak surface sound channel that might be enhanced during very calm ocean surface conditions.

Another distinctive sound that was detected is a 30-kHz spectral peak that is consistent with the echo-location click of beaked whales (*Johnson et al.*, 2004). This type of whale is pelagic (found only in deep water locations) and is difficult to detect visually as they spend most of the time diving underwater. This signal was present 1–2% of the time and was most often detected by the hydrophone at 200 m depth. This is the depth that *Johnson et al.* report that beaked whales begin clicking during deep dives. These whales are known to dive to depths below

1000 m and thus detections of this signal at 1000 m, and even occasionally at 2000 m, are consistent with beaked whales. There were no visual observations of whales during the experiment.

The main focus of the experiment was the detection of precipitation in deep water at different depths. In order to validate these detections, a dual-polarization, high resolution, X-band, coastal weather radar (XPOL radar) was located at Methoni, 17 km to the east of the mooring. Eight significant rain events were acoustically detected during the experiment (Table 1). Six of these events had partial or full radar coverage. All were confirmed by the weather station at Methoni, and all rain events recorded at Methoni during the experiment were detected acoustically. The radar data were used to verify the acoustic classification of rainfall, and the acoustic detection of imbedded shipping noise within a rain event (e.g., Fig. 18). Three simultaneous records of radar and acoustic rainfall measurements were compared to investigate averaging of the acoustic rainfall signal as a function of listening depth. These comparisons show an increase in effective listening area with increasing listening depth. The averaging radius for the radar data that resulted in the highest correlation with the rainfall measurement for the shallowest hydrophone (at 60 m) was between 450 m and 2 km, suggesting a listening area for the shallowest hydrophone of 1–12 km<sup>2</sup>. This is larger than expected (Fig. 3). In contrast, the averaging radius for the deepest hydrophone (at 2000 m) was 3–4 km, suggesting a listening area of 30–50 km<sup>2</sup>, less than expected (Fig. 3). This result was clearest for the rain event on 8 March, an intense isolated squall line that passed over the mooring very rapidly (2–3 min with rainfall rates over 50 mm/hr). An interesting acoustical feature of this event was a ‘moment of silence’ just after the passage of the squall. All of the hydrophones recorded a brief drop in sound level, including a drop to a level below the prevailing background sound before or after the squall at 200 m. This suggests that the background sound production mechanism (breaking waves from wind) had been suppressed by the intense rain, acoustical evidence of ‘rain calms the seas’. There was no radar echo return at the ‘moment of silence’.

## 8. References

- Cox, T.M., et al., 2006: Understanding the impacts of anthropogenic sound on beaked whales, *J. Cetacean Res. Manage.*, 7, 177-187.
- Johnson, M., P.T. Madsen, W.M.X. Zimmer, N. Aguilar de Soto, and P.L. Tyack, 2004: Beaked whales echolocate on prey. *Proc. R. Soc. London B (Suppl.)*, DOI 10.1098/rsbl.2004.0208.
- Ma, B.B., and J.A. Nystuen, 2005, Passive acoustic detection and measurement of rainfall at sea", *J. Atmos. Ocean. Technol.*, 22, 1225-1248.
- Medwin, H., and C.S. Clay, 1998: *Fundamentals of Acoustical Oceanography*, Academic Press.
- Medwin, H., and M.M. Beaky, 1988: Bubble sources of the Knudsen Sea noise spectra", *J. Acoust. Soc. Am.*, 86, 1124-1130.
- Medwin, H., J.A. Nystuen, P.W. Jacobus, L.H. Ostwald, and D.E. Synder, 1992: The anatomy of underwater rain noise. *J. Acoust. Soc. Am.*, 92, 1613-1623.
- Nystuen, J.A., M.J. McPhaden, and H.P. Freitag, 2000: Surface measurements of precipitation from an ocean mooring: The underwater acoustic log from the South China Sea", *J. Applied Meteor.*, 39, 2182-2197.
- Nystuen, J.A., 2001: Listening to raindrops from underwater: An acoustic disdrometer, *J. Atmos. Ocean. Technol.*, 18, 1640-1657.
- Nystuen, J.A., and E. Amitai, 2003: High temporal resolution of extreme rainfall rate variability and the acoustic classification of rainfall, *J. Geophys. Res.-Atmos.*, 108(D8), 8378-8388.
- Nystuen, J.A., 2005: Using underwater sound to determine drop size distribution", in *Sounds in the Seas: Introduction to Acoustical Oceanography*, edited by H. Medwin, Cambridge University Press.
- Nystuen, J.A., 2007: Acoustic footprints of ocean climate, submitted to *J. Acoust. Soc. Am.*
- Vagle S, W.G. Large, and D.M. Farmer, 1990: An evaluation of the WOTAN technique for inferring oceanic wind from underwater sound. *J. Atmos. Ocean. Technol.*, 7, 576-595.

<b>REPORT DOCUMENTATION PAGE</b>			<b>Form Approved</b> <b>OPM No. 0704-0188</b>	
Public reporting burden for this collection of information is estimated to average 1 hour per response, including the time for reviewing instructions, searching existing data sources, gathering and maintaining the data needed, and reviewing the collection of information. Send comments regarding this burden estimate or any other aspect of this collection of information, including suggestions for reducing this burden, to Washington Headquarters Services, Directorate for Information Operations and Reports, 1215 Jefferson Davis Highway, Suite 1204, Arlington, VA 22202-4302, and to the Office of Information and Regulatory Affairs, Office of Management and Budget, Washington, DC 20503.				
<b>1. AGENCY USE ONLY</b> (Leave blank)		<b>2. REPORT DATE</b> July 2007		<b>3. REPORT TYPE AND DATES COVERED</b> Technical Report
<b>4. TITLE AND SUBTITLE</b>  Spatial Averaging of Oceanic Rainfall Variability Using Underwater Sound. Ionian Sea Rainfall Experiment 2004: Acoustic Component			<b>5. FUNDING NUMBERS</b>  NSF Grant #0241245	
<b>6. AUTHOR(S)</b>  Jeffrey A. Nystuen, Eyal Amitai, Emmanuel N. Anagnostou, and Marios N. Anagnostou				
<b>7. PERFORMING ORGANIZATION NAME(S) AND ADDRESS(ES)</b> Applied Physics Laboratory University of Washington 1013 NE 40th Street Seattle, WA 98105-6698			<b>8. PERFORMING ORGANIZATION REPORT NUMBER</b>  APL-UW TR 0701	
<b>9. SPONSORING / MONITORING AGENCY NAME(S) AND ADDRESS(ES)</b> Eric C. Itsweire Physical Oceanography Program Division of Ocean Sciences, Room 725 National Science Foundation 4201 Wilson Blvd, Arlington, VA 22230			<b>10. SPONSORING / MONITORING AGENCY REPORT NUMBER</b>	
<b>11. SUPPLEMENTARY NOTES</b>				
<b>12a. DISTRIBUTION / AVAILABILITY STATEMENT</b>  <i>Approved for public release; distribution is unlimited.</i>			<b>12b. DISTRIBUTION CODE</b>	
<b>13. ABSTRACT</b> (Maximum 200 words)  An experiment to evaluate the inherent spatial averaging of the underwater acoustic signal from rainfall was conducted in the winter of 2004 in the Ionian Sea southeast of the coast of Greece. A mooring with four passive aquatic listeners (PALs) at 60, 200, 100, and 2000 m was deployed at 36.85°N, 21.52°E, 17 km west of a dual-polarization X-band coastal radar (XPOL) at Methoni, Greece. A dense rain gauge network was set up in Finikounda, 10 km east from Methoni to calibrate the radar. Eight rain events were recorded during the deployment; six of these events were recorded by both the PALs and the XPOL radar. The acoustic signal is similar at all depths and rainfall was detected at all depths, although the deeper PALs suffered an unexpected sensitivity loss and consequently did not trigger into high sampling mode as often as the shallower PALs. The total accumulation reported is lower for the deeper PALs. The acoustic signal is classified into wind, rain, shipping, and whale categories. The shipping signal increased throughout the deployment. A signal from whales is present roughly 2% of the time, most often at 200 m, and is consistent with the clicking of deep-diving beaked whales, although there was no visual confirmation of whale presence. Acoustic co-detection of rainfall with the radar demonstrates the need to classify the rainfall signal in the presence of other underwater noises. Once detection is made, the correlation between acoustic and radar rainfall rates is high. Spatial averaging of the radar rainfall rates in concentric circles over the mooring shows highest correlations with increasing acoustic recording depth, verifying the larger inherent spatial averaging of the rainfall signal with recording depth. For the PAL at 2000 m, the maximum correlation was at 3–4 km, suggesting a listening area for the acoustic rainfall measurement of roughly $\pi r^2 = 30 - 50 \text{ km}^2$ , in contrast to less than $3 \text{ km}^2$ for the acoustic measurement at 60 m depth.				
<b>14. SUBJECT TERMS</b> Passive acoustic monitoring, ocean rainfall measurement, Ionian Sea, Spatial averaging of rainfall, rainfall estimation, rainfall classification, ambient sound budget, beaked whales			<b>15. NUMBER OF PAGES</b> 47	
			<b>16. PRICE CODE</b>	
<b>17. SECURITY CLASSIFICATION OF REPORT</b>  Unclassified	<b>18. SECURITY CLASSIFICATION OF THIS PAGE</b>  Unclassified	<b>19. SECURITY CLASSIFICATION OF ABSTRACT</b>  Unclassified	<b>20. LIMITATION OF ABSTRACT</b>  SAR	